Variations of Mixed Layer Properties in the Norwegian Sea for the Period 1948–1999

J. Even . Nilsen[1235], Eva Falck[46]

[1]*Geophysical Institute, University of Bergen, Norway*

[2]*Nansen Environmental and Remote Sensing Center, Bergen, Norway*

[3]*Bjerknes Centre for Climate Research, Bergen, Norway*

[4]*Alfred Wegener Institute for Polar and Marine Research, Bremerhaven, Germany*

Progress in Oceanography, 2006, 70(1), p. 58–90, doi:10.1016/j.pocean.2006.03.014.

Abstract

The mixed layer of the ocean and the processes therein affect the ocean's biological production, the exchanges with the atmosphere, and the water modification processes important in a climate change perspective. To provide a better understanding of the variability in this system, this paper presents time series of the mixed layer properties depth, temperature, salinity, and oxygen from Ocean Weather Station M (OWSM; 66°N,2°E) as well as spatial climatologies for the Norwegian Sea. The importance of underlying mechanisms such as atmospheric fluxes, advective signals, and dynamic control of isopycnal surfaces are addressed. In the region around OWSM in the Norwegian Atlantic Current (NwAC) the mixed layer depth varies between ∼20 m in summer and ∼300 m in winter. The depth of the wintertime mixing here is ultimately restrained by the interface between the Atlantic Water (AW) and the underlying water mass, and in general, the whole column of AW is found to be mixed during winter. In the Lofoten Basin the mean wintertime mixed layer reaches a depth of ∼600 m, while the AW fills the basin to a mean depth of ∼800 m. The temperature of the mixed layer at OWSM in general varies between 12°C in summer and 6°C in winter. Atmospheric heating controls the summer temperatures while the winter temperatures are governed by the advection of heat in the NwAC. Episodic lateral Ekman transports of coastal water facilitated by the shallow summer mixed layeris found important for the seasonal salinity cycle and freshening of the northward flowing AW. Atmospheric freshwater fluxes have no significant influence on the salinity of the AW in the area. Oxygen shows a clear annual cycle with highest values in May–June and lowest in August–September. Interannual variability of mixed layer oxygen does not appear to be linked to variations in any of the physical properties of the mixed layer.

1 Introduction

Understanding and monitoring the seasonal cycle of the mixed layer in the Norwegian Sea and its interannual variability is of key importance to enhance our knowledge about the Atlantic flow towards the Arctic. An understanding of the processes by which the mixed layer properties vary is essential for quantitative diagnostics for the coupled ocean and atmosphere system and its effect on biogeochemical cycles and ecosystems. Seasonal and interannual fluctuations in the upper ocean climate are also of great importance in other aspects like biological production (Polovina, Mitchum, and Evans, 1995). Knowledge of the variability in the mixed layer and its properties in the Norwegian Sea is for instance highly important in the context of heat release from the Norwegian Atlantic Current (NwAC), which is the most important contribution of oceanic heat transport toward high latitudes in the Northern Hemisphere. The Ocean Weather Station M (OWSM; 66°N,2°E) has been operating for more than 50 years in the Norwegian Sea. Being strategically placed in the western branch of the northward flowing NwAC (Figure 1) OWSM is a unique place to monitor possible climatic fluctuations (Gammelsrød, Østerhus, and Godøy, 1992). The long time series that now exists from OWSM provides an excellent means to analyse variations in mixed layer properties for this area over different time scales.

[5]Corresponding author. Tel: +47 55205881; fax: +47 55205801; Email: even@nersc.no (J.E.Ø. Nilsen)

[6]Present address: Geophysical Institute, University of Bergen, Allégt. 70, N-5007 Bergen, Norway

The mixed layer (ML) is defined as a surface layer where there is nearly no variation in density with depth, i.e. a quasi homogeneous region (Kantha and Clayson, 2000). This homogeneity is caused by turbulence through the action of surface forcing, like mechanical mixing by wind stress and convective mixing by surface buoyancy fluxes. The mixed layer can often show a strong diurnal cycle (Brainerd and Gregg, 1995), with night-time convection due to cooling driving active mixing from the surface to the seasonal pycnocline, while during daytime a shallower restratification may occur due to heating. Salinity may also be of importance to mixed layers, especially after heavy rainfall when pools of freshwater at the surface can generate strong haloclines at their base (Lukas and Lindström, 1991), which can suppress mixing. We find Niiler and Kraus (1977) to provide most extensive and practical inputs on these issues. More recent is the book by Kantha and Clayson (2000), which gives a good introduction to the mechanisms that govern the depth and properties of the mixed layer. Spatial and monthly variability of the mixed layer depth (MLD) for the global ocean is provided and examined by Kara, Rochford, and Hurlburt (2003). However, their paper does not cover any part of the Arctic Mediterranean. Apart from the work done by Johannessen and Gade (1984), who used a one-dimensional model to simulate variations in MLD at OWSM for a 17 day period of March 1967, little has been done in the context of studying the evolution and variability of the mixed layer in the Norwegian Sea.

Since the start of hydrographical observation at OWSM in 1948, several papers have been written to understand the seasonal and interannual variability in the region and its underlying causes. Seasonal variations of temperature and salinity in the upper layer from 1948 to 1958 have been studied by Helland (1963) and annual variations of energy exchange across the air–sea interface for the same period by Bøyum (1966). Leinebø (1991) has looked at the oxygen variations in the intermediate water from 1953 to 1990. The long time series has been used by Østerhus and Gammelsrød (1999) to show that the temperature of the deep water at OWSM has increased considerable during the 1990s, while Blindheim, Borovkov, Hansen, Malmberg, Turrell, and Østerhus (2000) showed a long term decrease in both temperature and salinity in the upper 500 m of the water column. Furevik, Bentsen, Drange, Johannessen, and Korablev (2002) have used the OWSM data in their study of the temporal and spatial variability of the sea surface salinity in the Norwegian Sea. Time series of temperature and salinity anomalies for selected depths are presented in Gammelsrød and Holm (1984) for the years 1948–1981 and in Gammelsrød et al. (1992) for 1948–1991. Series from all depths for 1948–1999 are presented in (Nilsen, 2003).

In contrast to these earlier time series studies of the OWSM data, which were applied to fixed depths, we will in this paper present time series of mixed layer averages of temperature and salinity, together with time series of MLD and mixed layer averages of oxygen for OWSM as well as winter and summer climatologies for the Norwegian Sea. When considering the hydrographic conditions in the area of OWSM, with a frequent vertical movement of the transition layer between the Atlantic Water (AW) and the intermediate waters below (Mosby, 1962), an anomaly at a fixed depth may be the result of waters having different origins and consequently of different properties and therefore not represent a variability in time of the water mass under consideration. We believe that time series of integrated properties over the mixed layer give a more ideal picture of the variability of the AW than time series of properties from fixed depths. In this respect, ML-averages provide more reliable basis for creating spatial averages from oceanic stations, since the bulk of the mixed layer is taken into account and not only the highly variable surface measurements.

The climatologies of ML-properties are compared to relevant fields of atmospheric fluxes, in order to evaluate the importance of horizontal gradients in the area. For the annual cycle and interannual variations, the role of atmospheric forcing is examined, and effects of advection and entrainment are briefly discussed. Furthermore, the study describes some important mechanisms involving mixed layer processes through which the northward flowing Atlantic Water can be modified. The main objective of the present work is to show how different ML-properties in the Norwegian Sea vary on different time scales, and to reveal some of the underlying processes that cause such variations. The results (Section 6) have been divided into four sections treating the Mixed layer depth, ML-temperature, ML-salinity, and ML-oxygen separately. In each of these sections, the spatial and seasonal differences in the Norwegian Sea, the mean annual cycle at OWSM, and the multi-year time series from OWSM will be discussed.

Before the results are treated, we will present an overview of the current knowledge of the hydrography in the Norwegian Sea (Section 2), discuss important mechanisms governing the oxygen content of this part of the world oceans (Section 3), and account for the data (Section 4) and methods of analysis (Section 5) used in this paper.

2 Hydrographic conditions

The relevant hydrographical features of the Norwegian Sea will be described in this section. For a thorough description of circulation patterns and water mass modifications taking place in the whole of the Nordic Seas see Blindheim and Østerhus (2005).

Atlantic Water enters the Norwegian Sea through the Faroe–Shetland Channel and over the Iceland–Faroe Ridge (Hansen and Østerhus, 2000), and continues northward providing heat and salt to the Arctic Ocean (Figure 1). Between the Faroes and the Lofoten Basin, the two inflows mainly flow as separate branches, the eastern branch as a barotropic current along the Norwegian Continental Slope, the western branch as an unstable baroclinic jet originating from the Faroe Current and following the 2000 m isobath (Poulain, Warn-Varnas, and Niiler, 1996; Mork and Blindheim, 2000; Orvik, Skagseth, and Mork, 2001; Orvik and Niiler, 2002). Between the two branches the AW is strongly mixed and can thus be revealed as one warm and saline, "wedge" shaped water mass along the eastern side of the Norwegian Basin (Figure 2). Some AW is also found in the surface west of the western jet (Blindheim et al., 2000). The lower boundary of the AW ($T \approx 3$°C and $S=35$) is generally found at depths of about 400–500 m, from the continental slope to the position of the 2000 m isobath (Helland-Hansen and Nansen, 1909; Orvik et al., 2001), where it slopes upward and levels out at shallower depths before it rises to the surface further west.

This western border zone, where the AW meets the fresher and colder Arctic Water, is called the Arctic Front. This is an area with strong horizontal gradients. North of Jan Mayen this front is rather stably positioned, but in the southern part of the Norwegian Sea, relatively large shifts in its position occur due to variations in the volume of Arctic waters carried by the East Icelandic Current. Due to the constraint caused by these waters, the width of the Atlantic flow is relatively narrow here (Blindheim et al., 2000). This can be seen in Figure 3 which shows the mean seasonal variation in the extent of the AW as defined by the 35 isohaline surfaces. During summer the AW extends further to the west than in winter, but this seasonal difference can only be seen in the upper 150 m of the water column.

To the east of the NwAC, the coastal water of the Norwegian Coastal Current (NCC) is the dominant water mass (Figure 2) and is characterized by low salinity and seasonally variable temperature. Its western extension varies with season, reaching further west during summer than in winter. This can be seen in Figure 3 where the 35 isohaline surfaces along the coast of Norway give an indication of the horizontal and vertical variations in the extent of the coastal water. The NCC also becomes shallower in summer, possibly due to the seasonal maximum in coastal runoff which increases the density difference across the interface between the coastal water and the AW below and thus decreases its slope (Helland-Hansen and Nansen, 1909). The prevailing northerly winds in early summer introduce additional westward spread of the surface layer (Rey, 1981; Gade, 1986; Sætre, Aure, and Ljøen, 1988).

The upper layer of the Norwegian Sea in the area around OWSM is dominated by the warm and saline AW (Mosby, 1970), while the deep layers are filled with Norwegian Sea Deep Water, a rather homogeneous water mass in both temperature and salinity (Mosby, 1959). In between these two water masses the Arctic Intermediate Water (AIW) intrudes and is usually found at 500–800 m depth in the Norwegian Basin and 800–1200 m in the Lofoten Basin, and has its origin to the west of the Arctic Front (Blindheim, 1990). It is characterized by a local minimum in salinity and maximum in oxygen. The depth of the transition layer between AW and AIW at OWSM is known to vary considerably on short time scales, and may be found anywhere between 200 and 600 m (Mosby, 1950, 1962). Mosby (1962) examined the OWSM data from 1948–1957 and showed an extreme event in July 1949 where the depth of the transition layer had changed by 200 m in two hours. Due to the topographic steering (Svendsen, Sætre, and Mork, 1991) of the baroclinic western branch of the NwAC along the edge of the Vøring Plateau (Nilsen, 2004; Nilsen and Nilsen, 2003), the upward slope of the interface (Figure 2) only has a lateral variation in position of about 50 km (Smart, 1984). This is just where OWSM is situated, and the presence of the slanting interface has implications for the hydrographic record and the lateral variation in its position could be the cause of the variations seen in the depth of the transition layer. Both Sælen (1963) and Mosby (1970) revealed that eddy-like features were occasionally present in the NwAC with scales on the order of 50 km. These eddies could be stationary for several days or move with varying speed in a north easterly direction (Sælen, 1963). Such eddy-like features are associated with strong horizontal and vertical temperature gradients and may contribute significantly to the synoptic variations in temperature and depth of the transition layer.

3 Oxygen

The distribution of dissolved oxygen (hereafter referred to as oxygen) is governed by both physical and biological processes and the significance of the different mechanisms will vary both in time and space. Both processes cause an exchange of oxygen across the sea surface (Redfield, 1948). To make it easier to follow the discussions on oxygen later in this paper a short description of these processes is given below. Earlier studies of the annual cycle of oxygen from observed data in the Norwegian Sea can be found in Falck and Gade (1999) and Skjelvan, Falck, Anderson, and Rey (2001). Both studies showed that this region acts as a sink for atmospheric oxygen, which implies that heat loss, winter storms, and winter convection cause a higher oxygen uptake during winter compared to the oxygen released to the atmosphere due to heating and primary production in summer.

Biological activity affects the oxygen concentration of the upper ocean. During the process of photosynthesis oxygen is produced and released to the surface water, while respiration by organisms and decomposition of dead organic matter removes oxygen from the whole water column (Lalli and Parsons, 1997). Oxygen concentrations are normally higher in the euphotic zone (upper layer of the ocean where there is enough light for photosynthesis) during the productive season while below this layer decreasing concentrations are seen due to remineralization of organic matter.

There are several physical factors governing the concentration of oxygen in the mixed layer. Advection and diffusion redistributes oxygen at and away from the sea surface. Convection plays a major role in distributing oxygen input at the sea surface to deeper depths. Entrainment of waters from below, with a different oxygen concentration, can change the concentration of oxygen in the mixed layer. The transfer of oxygen between the atmosphere and the ocean plays an important role in modifying the concentration of oxygen in the surface waters. The difference between the oxygen concentration and the solubility concentration of oxygen in the surface water is the main parameter determining the amount and direction of oxygen transport across the air–sea interface. The solubility of oxygen in the surface water is a function of temperature, salinity, and pressure, but pressure is normally set to 1 atmosphere and the effects of salinity can be ignored (Colt, 1984), resulting in the solubility being inversely proportional to the temperature and seasonality in sea surface oxygen is expected to be correlated with the annual cycle of temperature.

The physical and biological factors described above result in a rather complex system governing the spatial and temporal distribution of oxygen in the upper ocean. Within the mixed layer, the oxygen concentration is often found to be close to the saturation concentration. Departures from this saturation concentration are the results of biological activity, surface heat fluxes, advection and turbulent diffusion, injection of oxygen by bubbles, and the rate of gas exchange. High supersaturation often occurs during the early summer when the rates of warming and primary production are highest. Surface cooling and entrainment of water with lower oxygen concentrations, due to mixed layer deepening during winter, often lead to undersaturation.

4 Data

The oceanographic observations of temperature and salinity at OWSM date back to October 1948, while measurements of dissolved oxygen started in 1953. The oceanic data sampling is done with Nansen bottles, equipped with reversing thermometers, around the standard depths of 0, 10, 25, 50, 75, 100, 150, 200, 300, 400, 500, 600, 800, 1000, 1200, 1500, and 2000 m. The program carried out at the station consists of daily casts (except Sundays) down to 1000 m and weekly down to the bottom. Temperature is read from the reversing thermometers. Salinity is analyzed ashore after each cruise, which has a duration of about a month. The storing time of the water samples are therefore normally about one to two months, but much longer storing times have occurred. This affects the salinity due to evaporation during storing and causes an additional error in the data. An effort to correct this has been made for the period 1980–1996, however only for depths larger than 1000 m (Mikki, 1998). Together with analytical errors and instruments of varying accuracy used during the years, this makes it difficult to estimate the precision of the salinity measurements. Oxygen is only measured once a week in the deep cast. The oxygen concentration of the water sample is analyzed on board using the Winkler titration method with visual detection of the titration end point, which generally gives a precision of the data of about 1%.

In this work temperature, salinity, and oxygen data from OWSM up to September 1999 have been used. Unfortunately some gaps of varying length exist in the sampling, the longest being about six months. During the early times the ship drifted a lot resulting in rather varying positions for the weather station (Nilsen and Nilsen, 2003). In this work we only include stations taken within the geographical limits of 65.5–66.5°N and 1–3°E, which are about ±50 km around the designated Weather Station position. Such a constraint is needed

in this area of strong lateral gradients associated with the sloping interface (Figure 2).

The following quality control was done on the data: For every density profile containing instabilities of more than 0.05 kg m^{-3}, the corresponding temperature and salinity profiles were visually inspected[1], and spikes subjectively regarded as prominent were removed from the dataset. Surface data of temperature and salinity are bucket and water intake samples. Therefore, they may be prone to additional errors due to less accurate thermometers used when measuring surface temperatures, compared to the reversing thermometers used in subsurface waters, and to inadequate rinsing of the bucket. Hence, surface data that showed extremely different density gradients compared to those from the measurements below were removed. Oxygen in the surface water is not measured, so the values at 10 m are used as surface values as well. Oxygen profiles that showed a clear offset from the mean deep water concentration were removed. The total number of profiles from OWSM used is about 10 000 for temperature and salinity and 1300 for oxygen.

To conduct the spatial study of the ML-properties in the Norwegian Sea, temperature, salinity, and oxygen from a database compiled at the Arctic and Antarctic Research Institute (AARI) in St. Petersburg (Johannessen, Alekseev, Ivanov, Korablev, Kovalevsky, Myakoshim, et al., 2000; Alekseev, Johannessen, Korablev, Ivanov, and Kovalevski, 2001; Furevik et al., 2002), were used. We have limited this part of our study to the area between 59°N and 72.5°N and east of 11°W (Figure 1). The data set consist mainly of data prior to 1990 and the subset used in this study contains about 50 000 profiles of temperature and salinity and about 15 000 oxygen profiles since 1948. Data are given at standard Levitus depths. Any missing surface oxygen data were replaced by the values from 10 m.

Monthly mean values at the surface of net short and long wave radiation, net fluxes of latent and sensible heat, precipitation, and six-hourly means of downward flux of momentum from January 1948 to September 1999, used in this work, are from the National Centers for Environmental Prediction/National Centers for Atmospheric Research (NCEP/NCAR) reanalysis data (Kalnay, Kanamitsu, Kistler, Collins, Deaven, Gandin, et al., 1996, hereafter referred to as reanalysis data). The spatial study uses gridded data (see open circles in Figure 1), while the temporal study takes its atmospheric series from the nearest grid point to OWSM (19 km south of the station). Observed wind data for every six hours from OWSM (15 m), since January 1949, and the coastal stations Ona and Sula on the west coast of Norway (10 m), since 1957, were provided by the Norwegian Meteorological Institute (DNMI).

5 Methods

5.1 Finding the mixed layer depth

Different methods for calculating the mixed layer depth can be found in the literature, and a thorough discussion of these as well as a search for an optimal approach has been given in Kara, Rochford, and Hurlburt (2000b) . The two main methods for finding the MLD are by use of a gradient criterion or a finite property difference criterion on density profiles[2]. A *gradient criterion* is defined as the depth where the gradient exceeds a given value, for density

$$\frac{\Delta\sigma_t}{\Delta z} = \left(\frac{\partial\sigma_t}{\partial z}\right)_C, \tag{1}$$

where $\Delta\sigma_t$ is the difference of the density anomaly ($\sigma_t = \rho - 1000$ kg m^{-3}) over a vertical distance Δz, and $(\partial\sigma_t/\partial z)_C$ is the specified gradient criterion (hence the subscript C). This criterion can only be used on profiles of high depth resolution, since the slope needs to be resolved. A *difference criterion* is usually defined as the depth where the property has changed by a certain amount from the surface value, for the case of density

$$\sigma_t(z) - \sigma_t(0) = (\Delta\sigma_t)_C \tag{2}$$

where $\sigma_t(0)$ is the value at the surface and $(\Delta\sigma_t)_C$ is the specified difference criterion. When using density as the variable (i.e. searching for the MLD), the criterion $(\Delta\sigma_t)_C$ can be defined directly or as a response of the equation of state to a given change in temperature in the surface (ΔT). The latter approach includes the nonlinear effects from the equation of state, as this yields different values for $(\Delta\sigma_t)_C$ depending on the surface temperature and salinity at the time of measurement (Glover and Brewer, 1988).

Kara et al. (2000b) promote an extension of this method by searching for a reference density at the base of a near uniform region, and then defining the MLD as the depth where a further density change corresponding

[1]The density criterion was chosen to avoid insurmountable number of graphs for visual control.

[2]The two criteria can also be used on temperature profiles to find the isothermal layer depth (ILD) which is not necessarily equal to the MLD (Kara, Rochford, and Hurlburt, 2000a).

to a given ΔT has occurred (found by linear interpolation). They found that the optimal criterion for the MLD in the North Pacific varied seasonally with higher ΔT during fall and winter, but conclude that using a MLD definition of ΔT=0.8°C should be applicable globally. Since the mixed layer can be considered to be near homogeneous, using any data within the layer (including the surface) in the difference criterion (2) is basically the same. It is merely a question of choosing a reference value for the (quasi) homogeneous region. Thus the recommended criterion (ΔT=0.8°C) should be independent of the reference level used. Brainerd and Gregg (1995), who examined both methods with several criterion values, found that a difference criterion gave more stable MLD estimates, but that the best value would vary under different conditions. From the above it is clear that one has to carefully choose the criteria to use, taking into consideration both the physical conditions at the study site and the context in which the mixed layer is studied.

The coarse depth sampling in the data used in this work exclude the use of a gradient criterion, so a suitable variant of difference criterion for density (2) was sought. We have chosen to find the MLD at single stations, not from smoother mean profiles, for two reasons: (i) We omit the extra process of interpolating the non-uniformly spaced samples from OWSM to common depths for the monthly means (Nilsen, 2003). (ii) It makes it easier to find a measure of uncertainty for the mean MLD in that we can use the standard deviations of the ensembles of single profile MLD values. Since the density variations in the upper water masses at OWSM are mainly determined by temperature variations (Johannessen and Gade, 1984) we have chosen to calculate the density criterion $(\Delta\sigma_t)_C$ as a response to a constant ΔT. Furthermore, this method gives a larger $(\Delta\sigma_t)_C$ in warm water than in colder water and thus follows the seasonal changes where the summer mixed layer has a stronger density difference to the water below than the winter layer. After different tests using the OWSM data, it was found that ΔT=0.8°C gave the highest success rate for finding the pycnocline proper (Nilsen, 2003). Note that this is the same as the global value suggested by Kara et al. (2000b).

The following steps were taken to identify the MLD: A density value corresponding to the MLD for each station was calculated by subtracting ΔT=0.8°C from the measured surface temperature, the depth of this base density was then found by linear interpolation in the density profile (Figure 4a). Density was calculated from temperature (T) and salinity (S) using the equation of state with no pressure dependence (Fofonoff and Millard, 1983, UNESCO 1983 (EOS 80) polynomial). Although both Brainerd and Gregg (1995) and Kara et al. (2000b) recommend the use of different ΔT values for different seasons, we think it is better to use the same value throughout this study. This definitely applies for the long time series study where it would complicate matters to introduce a seasonally changing value. The spatial study for the two separate seasons could perhaps benefit from an optimization of ΔT used in each season, but this would prevent good comparisons with the time series.

In profiles where instabilities stronger than 0.02 kg m^{-3} appeared at the surface, the first "stable" value found below was used as the surface value (Figure 4a). Regardless of their causes (measurement errors as well as physical effects) such instabilities represent a deviation from the values in the homogeneous region, and will result in too high reference densities and thus too deep MLD estimates. The inclusion of this restriction resulted in a significant lowering of MLD variability. Furthermore, in profiles where surface data were missing, the ∼10 m samples of temperature and salinity were used to calculate the reference density. This relaxation prevented unnecessary loss of MLD-estimates from otherwise useful profiles, which would have been the case if all profiles without surface data were discarded. Profiles that do not extend down to their calculated MLD density and profiles indicating instability at the depth where the calculated MLD density crosses the density profile, were discarded.

A large but certain error interval for the MLD estimates is the vertical distance to the nearest sampled data point in the profile. To ensure the MLD is not interpolated on the basis of data points that are too widely spread, MLD values were further discarded using the following criteria based on depth of the shallower neighbouring sample and accepted gap respectively: 0–100 m, 100 m; 100–300 m, 200 m; 300–500 m, 300 m; deeper than 500 m, 400 m. This resulted in a time series of about 8000 days with calculated MLD throughout the 51 year time span. Since the temporal gaps were many and often long, no temporal interpolation to create replacements for the missing days was attempted.

5.2 Calculating the averages

Every profile of temperature, salinity, and oxygen, from both the OWSM and the AARI dataset, was integrated vertically over the mixed layer and divided by the MLD to form bulk ML-values for the three ocean properties T_{ML}, S_{ML}, and O_{ML}. The required property values at the depth of the mixed layer (the base values) were found by linear interpolation. When calculating these ML-averages, temperature and salinity profiles with missing surface values were ignored. The integration was done by the trapezoidal method (Figure 4b). The same was

also done for percent oxygen saturation ($O^{\%}$) which had been calculated for each profile according to

$$O^{\%} = (O_{meas}/O_{sat}) \cdot 100\%, \tag{3}$$

where O_{meas} is the measured oxygen concentration and O_{sat} the oxygen saturation concentration calculated from the temperature and salinity data according to Weiss (1970).

The daily time series of MLD and ML-values are quite noisy and unevenly distributed in time. The noise is probably in many cases related to the frequent vertical movement of the water column as mentioned earlier. In addition, the time series are subject to errors from the method of MLD calculation and measurement errors of the profile data. To present a more stable and continuous time series, monthly mean values for each year were created, using profiles from within the calendar month. The average number of data in a month is N=12 (range 1 to 27) for temperature and salinity, and N=2 (range 1 to 5) for oxygen, thus some months do not have proper mean values. Due to this small and highly variable number of samples, we choose to use the sample standard deviation σ as an error estimate for the mean values (instead of the usual error estimate for the mean value: $\sigma_m^2 \approx \sigma^2/(N-1)$).

The vertical ML-averages from the AARI data were divided into sets for winter (Dec–Apr) and summer (Jun–Sept). The months chosen are the ones with deepest and shallowest MLD in the time series from OWSM, and the somewhat extended length of the two seasons are deliberately used to increase the number of estimates included. The resulting winter set consists of 15 000 MLD, temperature, and salinity estimates, and 3900 oxygen estimates, and the summer set of 22 000 and 7100 values, respectively. Bin-means in a grid of 2 by 1 degree bins centered on OWSM were calculated (points in Figure 1). Most bins contain more than 100 stations, but at some of the less important grid points the number can be as low as 10.

5.3 Forcing on the mixed layer

5.3.1 Heat and freshwater

The net heat flux from the ocean (Q in W m^{-2}) was calculated as the sum of net shortwave and longwave radiation and net fluxes of latent and sensible heat. The attenuation of radiation with depth was calculated for this area using the dataset of Rochford, Kara, Wallcraft, and Arnone (2001), and even for the shallow summer layers of the mean annual cycle, more than 98% of the incoming radiation was found to be absorbed in the ML. Only seven of the single months during the whole 50 year period have mean mixed layers shallow enough to let more than 10% radiation through. Thus the fraction of penetrative solar radiation to the water below the ML is generally ignored in this work. The evaporation (E) was calculated dividing the latent heat flux with a latent heat of evaporation of $2.5{\cdot}10^6$ J kg^{-1}. Precipitation (P) and evaporation are given in kg m^{-2} s^{-1}, which is the same as mm s^{-1}. The difference $E-P$ represents the net freshwater flux from the ocean. All these fluxes are defined as positive upward.

5.3.2 Buoyancy flux

The buoyancy flux (B in m^2 s^{-3}) was calculated according to Marshall and Schott (1999) as

$$B = \frac{g}{\rho}\left[\frac{\alpha}{c_w}Q + \rho\beta S_{ML}(E-P)\right], \tag{4}$$

where g is the acceleration due to gravity. Because of the strong temporal variability and horizontal gradients in the area, the density (ρ), the specific heat of seawater (c_w), the thermal expansion coefficient (α), and the haline contraction coefficient (β) are all considered functions of the hydrography (T_{ML} and S_{ML})[3]. The specific heat and density are calculated according to Fofonoff and Millard (1983) and the coefficients after McDougall (1987), all with zero reference pressure. The calculations do not, however, involve nonlinear operation with respect to these coefficients, since all averaging is done on each factor in (4) *before* calculating B. Since the heat capacity and density of water are much larger than those of air, vertical gradients in the water are insignificant in comparison, and thus bulk ML-temperature and salinity can be used instead of surface values (Niiler and Kraus, 1977). In addition, we find that the ML-values are less variable than the surface values, and thus give more robust mean values.

[3]One could argue that the relative variability of the coefficients and salinity are several orders of magnitudes less than Q and $E-P$, but they do in fact result in detectable differences in the spatial patterns of B. For temporal studies, the relative variability of the density is only one order of magnitude less than that of Q.

The summer and winter fields of T_{ML} and S_{ML} were interpolated linearly onto the reanalysis grid before calculating the oceanic constants. This means that the spatial study does not include any temporal variability of the oceanic values in (4) and the equation can be viewed as linear. Mean seasonal fields of atmospheric fluxes over the same months as the oceanic fields were used when calculating buoyancy fields for this study. In the temporal study at OWSM, the buoyancy fluxes were calculated using monthly mean values for all factors in (4). This means that nonlinear effects on time scales shorter than monthly is not accounted for, but given the significantly smaller variability of the oceanic components of (4) than the atmospheric, the nonlinearity is negligible.

5.3.3 Wind stress

The downward flux of momentum from the surface, the wind stress (τ_0) can be expressed by the friction velocity u_* (Niiler and Kraus, 1977):

$$u_*^2 \equiv \frac{\tau_0}{\rho}. \tag{5}$$

The friction velocity is the characteristic velocity scale for turbulent shear flows, and determines the velocity scale of turbulence and mixing in the mixed layer. According to Niiler and Kraus (1977) the work done by the wind on the mixed layer is proportional to u_*^3. The reanalysis provides momentum flux as two directional components, so to arrive at the absolute value for τ_0 and calculate u_*^3 by (5) requires nonlinear operation on the data. This nonlinear relationship is of some importance since the full effect of strong wind episodes (passages of storms etc.) of shorter duration than the sampling/averaging periods used, will not be accounted for.

For the time series study, wind stress data at a frequency of four times a day are used, and the nonlinear operations on this variable are applied at each time step before averaging further. This procedure should incorporate the effect of most storm passages. As was the case in the calculation of buoyancy flux (Section 5.3.2), the temporal variability (seasonal signal) of the density is not negligible in (5). The best available time series of density is that from the monthly mean S_{ML} and T_{ML}. Given the relatively slow changes of ocean properties compared to the atmospheric, we consider this to give sufficient temporal resolution for this value. Thus monthly estimates of u_*^3 are calculated using 6-hourly mean wind stress from the reanalysis data and monthly mean bulk ML-density by modifying (5) as follows:

$$\overline{u_*^3} = \overline{\left(\frac{\tau_0}{\rho}\right)^{\frac{3}{2}}} = \rho^{-\frac{3}{2}} \quad \overline{\tau_0^{\frac{3}{2}}}, \tag{6}$$

where the overline denotes a monthly mean. Due to the nonlinear nature of the wind forcing on the mixed layer we have not calculated mean seasonal fields for this value.

5.3.4 Stability

The most important factor that determines the effect of surface forcing on the mixed layer depth, is the stability of the water column itself. In homogeneous and stagnant water masses the surface forcing mentioned above will result in mixing to a depth proportional to the magnitude of the forcing. However, any layers with increasing stability will require stronger forcing to be mixed through. The rate of deepening of the mixed layer by erosion of a stable interface depends on how stable it is. The most commonly used variable for stability is the Brunt-Väisälä frequency (N) defined as

$$N^2 = -\frac{g}{\rho_0}\frac{d\rho}{dz}, \tag{7}$$

with ρ_0 as a constant reference density. The stability of the interface at the bottom of the mixed layer can be expressed by a discrete version of this function, namely the quasi-discontinuous change in buoyancy (b) across the base of the mixed layer (Niiler and Kraus, 1977),

$$\Delta b = -g\frac{\rho_1 - \rho_2}{\rho_0}, \tag{8}$$

where ρ_1 and ρ_2 is the average density of the mixed layer and the layer below, respectively. For the time series study Δb was calculated for each single station using a ρ_1 from S_{ML} and T_{ML}, and ρ_2 from T and S linearly interpolated to 150 m below the MLD. We have used a reference density of ρ_0=1027 kg m^{-3}, which is the mean density of the whole time series.

6 Results and discussion

The results obtained from the AARI-data give us the possibility to study the spatial and seasonal variability for a greater area of the Norwegian Sea before entering into a detailed interpretation of the time series from OWSM. In Figure 5 calculated mean winter and summer fields from the AARI-data of MLD, T_{ML}, S_{ML}, and O_{ML} for the Norwegian Sea are shown together with relevant atmospheric fluxes. The overall error estimates for the bin-mean values from the AARI-data are summarized in Table 1. The fields of buoyancy flux in Figure 5a and e are through (4) combinations of the heat- and freshwater fluxes (Figure 5b, c, f, and g). From a study of the different atmospheric fields (not shown), the thermal contribution to the buoyancy flux is found to be an order of magnitude larger than the haline, both in winter and summer.

Also shown in the panels of Figure 5 are the mean surface position of the 35 isohaline from the same hydrography. These isohalines define the separation of AW from the neighbouring water masses, Arctic Water to the west and coastal water off Norway (see also Figure 3), and in the following we will call the area inside these lines for the Atlantic Water domain (AW domain). Since OWSM lies inside this domain, our main focus in the following discussions will be on the AW.

6.1 Mixed layer depth

6.1.1 Spatial and seasonal differences in the Norwegian Sea

From the mixed layer depths in Figure 5a one can see that during winter the ML is deepest in the AW domain. This is expected, since the potential for heat loss and evaporation (and thus convection, see Equation (4)) is substantially larger in the AW than in the adjacent waters (Figure 3a, Inlays I–III vs. IV). Although the Norwegian Coastal Water is relatively warm (Figure 5b) its low salinity (Figure 5c) effectively prevents vertical mixing into the underlying AW through increased stability between the two water masses (Figure 3a, Inlay VI). Note that the MLD in the coastal water seems to increase away from the coast, in opposition to the notion of the Norwegian Coastal Current as a wedge shaped current. This is merely a result of averaging profiles from the frontal zone between the coastal water and the AW, which is neither stationary nor particularly sharp (Johannessen, Svendsen, Sandven, Johannssen, and Lygre, 1989).

Inside the AW domain the mixed layers during winter are shallower in the southern Norwegian Sea than further north. In the eastern Norwegian Basin MLD estimates are around 300 m with decreasing values westwards. When the NwAC reaches the Vøring Plateau area at 65°N the two branches of the current diverge to each side of the plateau due to topographic steering (Figure 1). There is an increase in MLD where the current enters the plateau (Figure 5a). An explanation for this can be that the divergence of the branches leads to longer residence times over the Plateau (as reported by Poulain et al., 1996), enhancing overturning and entrainment here. As the AW flows from the Vøring Plateau and into the Lofoten Basin, it both widens to fill the entire basin and deepens its vertical extension (Mork, 2006), implying even longer residence times here (Mauritzen, 1996a; Poulain et al., 1996). The mean winter MLD calculated in the Lofoten Basin reaches 520 m.

In addition to longer residence times of AW in the northern part, the heat loss to the atmosphere will influence the convection depth. Bunker (1976) showed that atmospheric heat loss is strong in the Lofoten Basin and Ivanov and Korablev (1995a; 1995b) described convective activity down to 800 m in the Lofoten basin, in the form of a mesoscale anticyclonic vortex (thermohaline anomaly observed in 300–1000 m) which was maintained and enhanced by wintertime convection within a basin wide cyclonic motion field. Such convection in this area can therefore provide mixing down to the interface with the AIW underneath.

In fact, the similarities of the winter MLD-field (Figure 5a) with the depth of the AW/AIW interface, as represented by the 35 isohaline surface in Figure 3a, indicate that the mixing depth in the AW domain is ultimately restrained by the strong density gradient found at the interface. The wintertime MLD in the AW domain will then be representative of the vertical extent of the Atlantic Water. When the entire AW column is mixed through like this, the MLD is not only affected by surface forcing, but also by other mechanisms that may control the interface depth. As Mosby (1974) pointed out, mixing across the interface transforms deeper water into AW, but the resulting deepening of the transition layer is counterbalanced by advection of bottom (and deep) water. Furthermore, in some areas the volume transport and dynamics of the AW flow may also control the depth of the interface. For instance, near OWSM in Figure 5a it can be seen that the wintertime MLD outlines the sloping pycnocline associated with the baroclinic western branch of the NwAC (Nilsen and Nilsen, 2003), and is thus likely to be affected by the dynamics of this flow. That the topographically controlled branches of the NwAC can determine the shape of the Atlantic Water's lower boundary is reflected in Figure 5a where the deepest MLD values reside over the deepest parts of the basin rather than coinciding with maximum

buoyancy flux.

In the western part of the Norwegian Basin features of the general circulation is also reflected in the spatial distribution of wintertime MLD. The tongue of deep MLD seen south of Jan Mayen is due to a returning branch of AW (Read and Pollard, 1992), while the tongue of shallow MLD stretching into the Norwegian Basin from the west is the Arctic Water of the East Icelandic Current. Where their paths cross, the East Icelandic Current spreads its fresher water over the returning AW, as indicated by the subsurface salinity maximum in Inlay III of Figure 3a.

The summer MLD in the Norwegian Sea is generally between 20 and 40 m (Figure 5e), which is about one 10th of the winter values. The deepest mixed layer depths are found in the Lofoten Basin and especially in the AW inflow area around the Faroe Islands. The overall buoyancy forcing has a stabilizing nature (negative) during summer. Compared to the adjacent waters, the buoyancy fluxes over the AW domain are smaller, the result of which is a deeper ML there. This is especially seen in the match between the increasing MLD northward of 66°N and the minimum in buoyancy input from the atmosphere. However, the shallow MLD between 64–66°N represents an exception in this respect. The pattern of buoyancy fluxes reflects the minimum in oceanic heat gain north of OWSM (Figure 5f) as well as the positive net atmospheric freshwater flux around OWSM (Figure 5g) to be discussed later.

6.1.2 Temporal variability at OWSM

The mean annual cycle of MLD at OWSM shows a summer mixed layer of about 20 m, and depths shallower than 50 m is seen from June through September (Figure 6a). From the figure it is clear that the development of the summer mixed layer happens rather quickly some time between April and June, whereas the mixed layer deepening in autumn takes much longer time (Sept–Jan). This is, of course, due to the fact that the mechanisms behind these two transitions are fundamentally different. From the temperature profiles in Figure 7a and e (which are inversely representative of the mean profiles in density) it can be seen that the development of a shallow thermocline (pycnocline) only requires heating of the surface waters in contrast to the deepening phase which requires erosion of the pycnocline. The latter normally happens as episodic deepening during storm passages assisted by convection due to surface cooling. By the end of the winter (Jan–Mar) the mean MLD is found between 250–280 m.

Figure 6a also reveals that the year to year variability of MLD is much higher during winter than during summer. This variability can be connected to the dynamics of the NwAC and the underlying waters, as well as to the variable surface forcing on the mixed layer. In the time series of monthly mean MLD at OWSM (Figure 8) the annual cycle as well as the interannual variability is clearly seen.

Deepening

In August–September, the input of buoyancy from the atmosphere (heating) ceases and the turbulence from the wind can start to erode the base of the shallow summer mixed layer. At the same time the intensity of the wind mixing also tends to increase and eventually reversed buoyancy flux initiates convective mixing. The erosion of the strong summer pycnocline depends on the strength and persistence of these two forcing mechanisms. To investigate how these mechanisms work on the deepening of the mixed layer bar graphs are plotted in Figure 8, where the open bars above the MLD-curve represent convective forcing and filled bars represent wind mixing. Each year around September, or sometimes earlier, the filled bars increase their length while the open bars switch from upward to downward. As soon as "downward forcing" dominates there is always some increase in MLD. However, the initial deepening of the layer is not seen to be proportional to the strength of the atmospheric forcing. Some years the deepening is weak although the bars are relatively long. This shows that the forcing needs more time to erode the base of the mixed layer, and the longest delays will be discussed at the end of this section.

Since the month to month deepening of the mixed layer can be expected to be roughly proportional to the amount of forcing acting on the layer, we will examine how much of the observed ML-deepening can be explained by surface forcing. A relation for deepening of the mixed layer (i.e. the entrainment velocity w_e) is expressed by Niiler and Kraus (1977) as

$$\frac{dh}{dt} = w_e = \frac{2mu_*^3}{h\Delta b} + \frac{nB}{\Delta b} \quad \text{for} \quad B > 0, \tag{9}$$

where h represents the MLD, and m and n are proportionality factors. A multiple linear regression of the two forcing terms in (9) on the observed changes in MLD was performed. The predictors were calculated from monthly values of atmospheric forcing and stability, multiplied by a dt of one month. The observed changes in

MLD (ΔMLD) during calendar months were calculated as differences between monthly means centered on the 1st of each month. Only data from months with a deepening mixed layer were used. Limiting the regression to data from months with mean MLD less than 180 m gave r^2=0.75. This means that most of the month to month deepening down to this depth can be explained by atmospheric forcing through this regression model (9). When data from deeper mixed layer cases were included the result was a poorer correlation. The cause for this is that the deeper MLD values are closer to the ultimate winter depths of the mixed layer, i.e. have reached the dynamically controlled base of the Atlantic layer.

The relation between the proportionality factors m and n reflects the relative importance of the two forcing terms in (9). The factors found by this regression were m=0.32 and n=1.00. It is expected that they are functions of depth (Niiler and Kraus, 1977), and using only data from shallower ML-depths resulted in smaller n (to n=0.63 when MLD<30 m) while m stayed approximately constant around 0.30. This means that the proportionality to h^{-1} in (9) is an applicable first approximation of the depth dependency of the wind forcing.

Winter depths

The depth of the mixed layer in each winter is highly variable on both monthly and shorter time scales, as can be seen in the month to month variations and the large standard deviations in Figure 8. In addition to these intra seasonal variations there are large year to year differences. The mean winter depth is around 280 m, but the winters of '57–'60, '62, and '93–'95 have overall MLD closer to 200 m, while in the winters of '49, '70, '71, '92, and '97 it is closer to 400 m. There may be different causes for this interannual variability. First of all the convective forcing needs to be sufficiently strong and persistent during autumn and winter. Qualitatively, this can be studied for the different years in Figure 8 by comparing the length and duration of downward bars with the wintertime MLD. However, the variability of maximum or overall winter MLD does not seem to be related to the variations in surface forcing.

Another cause for the wintertime variability of the MLD could be the dynamics of the NwAC, as discussed in the beginning of this section. To examine this issue, linear interpolation has been applied on the single profiles to find the depths at which S=35, and monthly mean values of these depths are shown as small circles in Figure 8. These depths are per definition representative for the vertical extent of the AW. A comparison of this depth with the estimated MLD can maybe give some answers about the variability of the winter MLD. The mean depth of S=35 through the whole period is around 300–400 m, but there are periods that deviate from this. In the years '57–'59 and '93–'96 the mean depth of the AW was between 200 and 300 m, while the period '69–'73 is characterized by deeper values (many even below 500 m). It is in the periods of shallow AW most of the shallow winter mean MLD values occur, while the period of deep AW has two of the deepest winter mixed layer observations.

This combined time series of both MLD and S=35 (Figure 8) indicates that the transition layer underneath the AW impedes the atmospherically forced deepening and may even limit the ultimate depth of the winter mixed layer. Generally, the depth of S=35 lies some 50–100 m below winter MLD values. This relation is expected when the MLD has reached the transition layer, since our MLD estimates represent the top of the pycnocline, and thus lies above the middle of the transition zone. Thus it seems that the AW is well mixed down to its base in most winters. Also on shorter time scales (month to month within winters), the MLD is seen to follow the depth of S=35. There is a correlation of r=0.68 between the depth of S=35 and MLD values deeper than 180 m from the daily profiles at OWSM (N=2117, not shown). Good visual examples of such covariance over several months are the winters of '56 and '80 (Figure 8). In such winters it is more evident that the MLD has reached the transition layer and that it is this layer that constitutes the base of the winter mixed layer.

Whether it is erosion due to convection or dynamical variations of the transition layer that determines the overall MLD during winter, is hard to assess and likely to vary for different periods. However, on monthly and shorter time scales there is no significant correlation between the winter MLD and the atmospheric forcing (as discussed in relation to the deepening mixed layer). Since OWSM is situated above the unstable sloping interface between the AW and the Arctic Intermediate Water (Dickson, 1972; Nilsen, 2004; Nilsen and Nilsen, 2003), it is more likely that the short term winter variability in MLD is due to the movements of this interface rather than the slower convective processes.

Restratification and the summer season

The onset of surface heating in spring and the following restratification occurs rather quickly between April and June. Small differences in the timing of the restratification can be seen, as indicated by the year to year differences in May MLD (marked with circles in Figure 8).

The depth of the developed summer layer is the result of a balance between the buoyancy input from the atmosphere ($-B$, mostly from heating) and the turbulent kinetic energy from the wind ($\propto u_*^3$), which erodes

the base of the mixed layer. The erosion is countered by the strength of the stability at the base of the mixed layer. In Figure 8 the bar graphs above the MLD-curve qualitatively show this balance.

Sometimes the mixed layer stays shallow even though the buoyancy flux has become destabilizing and the joint effect of the atmospheric forcings should result in deepening of the layer (as is the case for '53, '54, '56, '57, '69, '74, '78, '80, '84, '85, '87, '88, '90, and '94). Looking at the stability at the base of the mixed layer (the bar graphs below the MLD plot in Figure 8), it is clear that these summers have the most stable mixed layers. Since the simultaneous (on monthly time scale) input of buoyancy from the atmosphere is not sufficient to counter the wind mixing and maintain the shallow mixed layer, this stability must be provided by some other mechanism. This can be achieved by accumulation of heat or fresher water in earlier months, both from atmospheric fluxes and from lateral advection, as well as from lateral advection in the same month. All the above mentioned instances of high stability can be explained by looking for warm and fresh anomalies in the time series of ML-temperature and ML-salinity (Figures 10 and 12). These time series and the reasons for their extremes will be discussed in the next two sections. At this point it is sufficient to note that high ML-temperature and low ML-salinity alternate, and some years cooperate, in creating the extra stable summer layers in the years mentioned above.

6.2 Temperature

6.2.1 Spatial and Seasonal Differences in the Norwegian Sea

In winter, the highest ML-temperatures are found in the eastern part of the AW domain (Figure 5b). This shows that the area is dominated by the inflow of warm AW following the continental shelf and spreading out past OWSM and into the Lofoten Basin. Also shown in the same figure is the heat flux (Q) to the atmosphere, which is larger in the AW domain than in the neighbouring waters. The strongest gradient in Q is seen across the Arctic Front separating the AW from the Arctic Water. As the AW flows northward it is cooled, resulting in decreasing temperatures downstream. Furthermore, the increasing heat flux seen along the path, with maximum in the Lofoten Basin, enhances this horizontal ML-temperature gradient. Mauritzen (1996a,b) showed that the observed cooling of the NwAC can be explained by atmospheric heat loss alone, and that the net annual heat loss required is approximately 70 W m^{-2}. In comparison, this is equal to the annual mean heat flux at the position of OWSM, when calculated from the reanalysis data. The winter field of ML-temperature in the AW domain is also indicative of the density increase of the AW, which is 0.2 kg m^{-3} from south to north over the study area (calculated from the winter fields of T_{ML} and S_{ML}).

Over the whole area the summertime mixed layer is shallow and subject to atmospheric heating due to the dominance of insolation (Figure 5f). The warmest ML is seen along the coast of Norway, i.e. in the NCC. This is due to the shallowness of the ML in the coastal area causing the temperatures to become higher here than further off shore. In addition, warmer coastal water from the North Sea is advected into the area by the NCC. The result is seen in the ML-temperature field (Figure 5f), which shows a tongue of warm water spreading northward along the coast. The overall difference between mean summer and winter T_{ML} is quite uniformly 4°C, the spatial difference being limited to the east-west shift in the position of the maximum (Figure 5b vs. 5f). Thus the most prominent advective sources of warm water in the surface are the NCC in summer and the NwAC during winter.

6.2.2 Mean annual cycle at OWSM

The annual cycle of ML-temperature at OWSM (Figure 6b) shows that the coldest ML-temperatures are normally encountered during March, with a mean value of 5.9°C, and the warmest month is August with a mean temperature of 11.5°C. The interannual variability of ML-temperatures is greater during the summer months, i.e. ±1.5°C, compared to ±1.0°C in the winter. The onset of spring warming restratifies the water column from April to June. From the hysteresis curve in Figure 9a it can be seen that when the shallow summer mixed layer has developed, its depth decreases only marginally towards 20–25 m, but the layer is subject to further heating until August. From August to March the layer deepens and its temperature decreases, but quite slowly after January when the MLD is already near its mean winter maximum of 280 m.

The seasonal development of the vertical temperature distribution in the upper 300 m at OWSM is shown in Figure 7. The lower part of the AW is separated from the ML during summer and the warming from the atmosphere only affects the ML-part of the AW (Figure 7e). There is also a temperature increase in the lower part, most likely due to inflowing AW, until August. Then, during the deepening phase (Figure 7a), the temperature increase between 50 and 150 m is due to the surface heat being mixed into the lower part of the AW. However, this increase is small since the main forcing behind the mixing is heat loss to the atmosphere

(which cools the whole mixed layer). By December, the warm water of summer is completely mixed with the rest of the AW and further temperature decrease is uniform throughout this layer.

6.2.3 The 51 year time series at OWSM

The time series of monthly mean temperature in the mixed layer (Figure 10) clearly shows the annual cycle of heating and cooling, with mean summer values normally around 11°C and winter temperatures reaching down to about 6°C. The winter minima show little variability and no overall trend for the 51 years studied.

As shown in Figure 6b, the spring heating usually occurs from May to July, with ML-temperatures in June somewhere between 8°C and 10°C. The variability of the June temperatures can give an indication of how early the upper ocean is warmed in the different years, and thus these months are circled in Figure 10. Years with a warm June are usually the same as the ones with high maximum ML-temperatures. In some years the highest ML-temperature reaches above 12°C ('50, '53, '54, '69, '74, '80, '85, '88, '90, '91, and '94). The time of maximum ML-temperature is usually in August, but in some summers it is already in July ('51, '58, '72, '80, '84, '87, '98, and '99). The bar graph of Figure 10 indicates that the accumulated amount of atmospheric heating prior to the maxima is also larger in these years. The autumn cooling usually results in a colder September ML, but in the years '49, '51, '55, '58, '67, '73, and '95 the ML-temparature for this month remains near the maximum. All except the last of these delayed temperature drops seem to be due to atmospheric heating extending into September.

Although there seems to be a connection between the month to month changes in the ML-temperatures and the net atmospheric heat flux in Figure 10, which of course is reasonable, little more than the synchronicity of their annual cycles can be revealed from the time series plot. To further investigate the relationship between the temperature changes and the atmospheric input of heat at OWSM a linear regression model was set up. As a basis we used the following 1D model proposed by Niiler and Kraus (1977) for the temporal temperature change as a function of entrainment of water from underneath and surface heat flux:

$$\frac{dT_{ML}}{dt} = -\frac{w_e \Delta T}{h} - \frac{Q}{\rho c_w h}, \tag{10}$$

where ΔT here is the discontinuous temperature difference between the mixed layer and the underlying waters, and w_e is the entrainment velocity defined in (9). The first term on the right hand side of (10) is hard to quantify using monthly mean data, since using the change in MLD (dh) to calculate w_e, will not take into account episodes of entrainment on shorter time scales. On this basis, we have decided to let the cooling by entrainment be among the unknown factors and only use the heat flux term as a predictor for the regression. Consequently, we want to avoid the deepening periods between shallow summer and deep winter situations when entrainment is strong and deep vertical mixing processes prevail (see Figure 7 and Section 6.1.2). Furthermore, the relation (10) between the heat content of the ML and surface heat fluxes is not valid for the springtime situation when a new shallow summer mixed layer is formed in the upper part of the deep winter ML. Thus two regressions were done, one based on data from months with shallower ML than 65 m (motivated by best fit of the regression) and one for ML deeper than 200 m (deepest possible limit without loosing too much data and reducing the fit).

To make a linear regression model from (10) with the observed quantities temperature (T_{ML}) and MLD (h) as the response, a heat content of the mixed layer, E_{ML} in J m^{-2}, is introduced:

$$\frac{dE_{ML}}{dt} = \rho c_w h \frac{dT_{ML}}{dt}. \tag{11}$$

The surface heat flux to the mixed layer can then be regressed onto the measured change in heat content with the linear model

$$\frac{dE_{ML}}{dt} = b_0 - b_1 Q, \tag{12}$$

where b_0 and b_1 are regression coefficients. In this model, b_0 accounts for the constant balanced effect of heat sources other than Q, such as advection, entrainment, or eddy diffusion. The monthly change in ML-temperature (dT_{ML}) was calculated from a new set of T_{ML} values using monthly means centered at the 1st of each month to match the timing of the mean values of Q which are from the calendar months. The results of the regressions are shown in Figure 11.

For the deep mixed layer at OWSM (Figure 11a) the regression explains only 49% of the variance in temperature. The rest of the variance, the large scatter, is due not only to the uncertainty of the data, but also variability of the oceanic heat transports. The NwAC constantly provides heat to the deep winter mixed layer

at OWSM, and this is reflected in the constant b_0=241 W m^{-2}. The slope of the regression is b_1=1.8 which means that the atmospheric heat flux model underestimates the observed heating and cooling of the mixed layer. This steep slope of the regression can be explained by the seasonal variability of the heat content of the NwAC. Mork and Blindheim (2000) showed that in spring and summer there is a temperature increase in the AW advected to OWSM. As discussed in Section 6.2.2, the temperature increase in the core of the AW during late summer and fall is probably due to the mixing down of the warm shallow summer mixed layer. Thus the covariability of the advective and the radiative heating could be due to the effect of autumn mixing further upstream. In conclusion, the temperature of the deep winter mixed layer at OWSM can be said to be strongly influenced by the NwAC and the variability of its advective heat flux.

When the mixed layer is shallow (Figure 11b), the response of its heat content to the atmospheric warming is almost one to one (b_1=0.89), and the regression explains as much as 78% of the variance. In other words, the atmosphere determines the warmth of the summer mixed layer. The constant term b_0=39 W m^{-2} indicates that there is some leakage of energy from the shallow summer mixed layer. The mechanism behind this is most likely to be mixing with the colder waters below, both when the mixed layer is deepening and through episodic wind induced deepening while the mixed layer is getting shallower on a monthly time scale. Penetration of solar radiation to the waters below the ML would also represent a "leakage", but the fraction of months having shallow enough ML to let significant amounts of radiation through, is far too small to produce a constant term in the regression (see Section 5.3.1).

Regarding the year to year differences in the maximum summer temperature, it is possible to integrate (10) in time to express an expected long term temperature change due to atmospheric heating (neglecting the entrainment term). Through that expression a significant correlation of r=0.72 was found between the maximum summer temperature and the cumulative heat input since the start of the spring warming. Under the assumption that the interannual differences in winter ML-temperature is negligible, the interannual variability in maximum ML-temperatures can be said to be governed by interannual variability in the atmospheric heat fluxes.

Among other mechanisms that can control the heat content of the summer mixed layer are the previously mentioned entrainment from below, changes in the temperature of this entrained water (AW), lateral advection due to wind forcing (Ekman fluxes) in the summer, and also eddy fluxes from the lateral boundaries of the NwAC during both seasons. In the next section a relation is shown between wind driven transports of coastal water and fresh summer anomalies at OWSM. The same method was tested for temperature anomalies, but no significant relation to advection of warm coastal water (see Figure 5f) was found.

6.3 Salinity

6.3.1 Spatial and seasonal differences in the Norwegian Sea

The winter field of ML-salinity (Figure 5c) shows the intrusion of AW alongside of the Norwegian shelf break and the spreading of this water mass over the Vøring Plateau and into the Lofoten Basin. As mentioned above, during winter the AW is generally well mixed, from its base to the surface, thus the winter S_{ML} values can be viewed as representative of the whole column of AW. Characteristic of the salinity in the NwAC is a significant freshening (about 0.1 salinity units) as it enters and passes through the southern Norwegian Sea compared to the moderate freshening downstream. Looking at the winter fields of ML-salinity and net atmospheric freshwater flux they do not coincide well in the Atlantic domain (Figure 5c), thus precipitation and evaporation seem to have little influence on such a deep mixed layer.

During summer, the E and P patterns have the same features as in winter, but the fluxes are weaker. On the other hand, the shallow summer mixed layer is more receptive to changes by atmospheric freshwater fluxes, and the weak summer time maximum in ML-salinity seen north of OWSM can therefore be connected to the maximum in $E-P$ (Figure 5g). The distance between these two maxima is roughly two degrees latitude, over which the water needs about a month to travel (assuming a northward drift of 10 cm s^{-1}; e.g. Russenes, 1957; Mosby, 1970; Blindheim, 1993). During one month, a freshwater loss of 10 kg m^{-2} from a 28 m thick mixed layer can increase the salinity by 0.01, all of which are numbers compatible with the observations shown in the figure. In addition, the deepening of the layer downstream of OWSM (Figure 5e) implies admixture of saltier AW from below (see Figure 7f). For instance if a 28 m thick layer with salinity 35.1 deepens 4 m into a layer with salinity 35.2, the corresponding salinity increase will also be about 0.01. Although these numbers are only rough estimates, they show that the two effects can be equally important, as well as having orders of magnitude comparable with the observed change (<0.05).

6.3.2 Mean annual cycle at OWSM

Although the ML situation in the AW domain is completely different between the two seasons, at OWSM there is no appreciable difference in ML-salinity (Figure 5c,g). The annual mean ML-salinity at OWSM is around 35.1 and the annual cycle consists of a maximum in spring and minimum in late summer, having only a 0.05 deviation from the mean (Figure 6c). As can be seen, the summer minimum in this empirical cycle is mainly due to sporadic fresh anomalies.

During the first half of the autumn the ML-salinity increases (Figure 9) due to entrainment of the more saline AW under the summer ML and from Figure 7b it is clear that the deeper parts of the NwAC is freshened by the mixing with the surface layer. Quantitatively, vertical integration of the monthly mean profiles show that there is a close (to the order of 0.01 salinity units) salt mass balance between September and December, indicating that the amount of freshwater supplied from the surface layer is causing the observed 0.1 salinity unit freshening of the water underneath. This does not exclude the possibility of a balance between the salt flux of the NwAC and downward or lateral diffusion out of the current, but it is interesting to note that the strongest freshening *along* the NwAC is of the same order of magnitude (Figure 5c) and occurs in the southern area where the freshwater layer is seen to develop in summer (Figure 5g). Furthermore, the end product of the vertical mixing has a salinity a little above 35.1, which is seen to persist in the current far into the northern regions of the study area (Figure 5c). By December, the Atlantic layer at OWSM is homohaline, and the fresh layer has disappeared (Figure 7b). Further deepening of the mixed layer is accompanied by a salinity increase in the upper 200 m, caused by the saline inflow from the Atlantic Ocean. However, since the mixed layer deepens and salinity decreases with depth, this small increase is not reflected in the ML-salinity until February–March (Figure 9b).

This advection of saline AW to the OWSM area dominates the ML-salinity during the early part of restratification, but by June the mixed layer becomes shallow enough to facilitate wind driven transports from the fresher waters neighbouring the NwAC, or to have its salinity influenced by atmospheric freshwater fluxes. As can be seen in Figure 7f, the upper 50 m freshens considerably from May to August. Thus the ML-salinity increases from March to May, and then decreases toward August (Figure 9b). The core of the NwAC will, after restratification has taken place, lie below the MLD, and is therefore "detached" from the mixed layer and hence from direct atmospheric influence. In contrast to the freshening seen in the ML, the salinity in the core continues to increase until July and a maximum in salinity is seen around 50–100 m during summer (Figure 7f).

Note how the surface accumulation of heat and freshwater during summer and subsequent deep mixing during autumn impose an annual cycle in both temperature and salinity of the NwAC as a whole. From Figure 7 it is clear that time series from the NwAC core around 100 m depth will have salinity maximum in July-September and minimum in December, while the temperature cycle at this depth will lag salinity by three months. The same timing of the cycles was shown for the Svinøy Section (Mork and Blindheim, 2000, their Figure 17a).

6.3.3 The 51 year time series at OWSM

The time series of ML-salinity (Figure 12), contrary to temperature (Figure 10) and oxygen (Figure 14), shows no strong annual cycle (see also Figure 6). The winter salinity values (e.g. circled January months in Figure 12) are usually quite stable since they represent the deep column of AW. There are, however, some long term changes in this winter salinity, which reflect variations in the salinity of the NwAC. The most prominent is the "Great Salinity Anomaly" ("GSA '70s" Dickson, Meincke, Malmberg, and Lee, 1988) which was seen at OWSM in the second half of the 1970s (Gammelsrød et al., 1992). This can clearly be visualized in the time series although there is a gap of six months in the data around the time when the GSA was at its strongest at OWSM. Belkin, Levitus, Antonov, and Malmberg (1998) have identified another anomaly ("GSA '80s") passing through the Norwegian Sea in the years '87–'88, and they also point to a "GSA '90s" (Belkin, 2004). However, these anomalies did not have the same strength nor the deep vertical extension as the GSA '70s had at OWSM (Nilsen, 2003, his Figure A.1), and they are thus not so easily recognisable in our ML integrated salinities.

In most years a freshening of variable strength takes place in the summer mixed layer. Gammelsrød and Holm (1984) found that in the years '51, '57, '62, '65, and '78 very low salinities were present at the surface. They attributed this to either the formation of the shallow summer mixed layer, which would limit the diluting effect of the precipitation to the surface layer, or as a consequence of advection and horizontal diffusion. From our time series, the years '74, '84, '85, '87, and '88 can be added to this list.

The net local surface freshwater flux at OWSM is dominated by evaporation (Figure 12), and thus the freshening events cannot be explained by local atmospheric freshwater fluxes. This strong relation between evaporation and freshening, seems counterintuitive. However, evaporative maxima in this area can be expected

to occur when colder and dryer air masses enter from the north, and northerly winds can drive Ekman transports of fresh coastal water into the Atlantic domain. Helland (1963) demonstrated a connection between the wind forcing over the coastal water southeast of OWSM and the surface salinity minima occurring at the station. Following Helland, wind data at OWSM and coastal winds, averages of stations Ona and Sula, were averaged to form a representative wind for the region. The northward component of this wind is then integrated during the development of each salinity minima at OWSM (Figure 12). This integrated wind component represents the wind driven transport in the Ekman layer toward the coast, and is compared to the corresponding minima of monthly mean ML-salinity in Figure 13. Although the spread of data is severe, an inverse relation can be seen, and it is evident that the strongest minima have developed under the influence of northerly winds (negative values) producing an Ekman transport of fresher water away from the coast and into the NwAC. A linear regression of the wind-days on the minimal salinities explains 46% of the variance in these values (not shown), which is not small given the indirect and coarse nature of the model.

Hydrographic sections along 66°N in the AARI-database, coinciding with minima at OWSM, give further support for the connection to the coastal water by revealing surface water of S<34.9 stretching toward OWSM from the east (inlay of Figure 13). The timing of these sections is not necessarily at the most extreme minima at OWSM, but within the period of low salinity (for instance the 34.9 isohaline in the section from '77 does not reach west of OWSM although the salinity at the station goes below 34.9). These isohalines must be studied with utmost caution since they are the result of interpolation on a sparse dataset. Still the wind study and the sections leave little doubt that the strong salinity minima at OWSM are results of freshwater from the coastal regions.

There are several sources supporting this view. In a study of all nine North Atlantic Ocean Weather Stations, Taylor and Stephens (1980) pointed to the irregularity of the surface salinity cycle and its deviation from the direct atmospheric forcing, and concluded that the salinity cycle is influenced by horizontal turbulent diffusion and advection. Mauritzen (1996a) concluded that the freshening of the NwAC along its path, over its whole lateral extent, can be explained by admixture from the NCC. In Figure 3b one can see from the mean summer 35 isohaline surface that fresh coastal water in summer stretches out far from the coast toward OWSM. In general this has to do with the summer maximum in coastal runoff, but it is not likely to be a sufficient explanation for significant freshening as far west as at OWSM. Sætre et al. (1988) discussed the reasons for the seasonal displacement of the NCC, and held forth northerly winds in the summer as the most prominent explanation. Although concentrating on the North Sea, they demonstrated Ekman transport and coastal upwelling in response to these winds also along the whole western coast of Norway. Their case study concerned a wind driven widening of the NCC in the summer of '84, which had "the strongest and most persistent northerly winds ... since 1965". The period between these years is lacking severe salinity minima also at OWSM (Figure 12).

Although local net freshwater flux from the atmosphere is not responsible for the strongest salinity extrema at OWSM, the mean net atmospheric freshwater fluxes for the area show that precipitation is more pronounced in the regions outside of the NwAC (Figure 5g). The variations in precipitation are also stronger here in the source areas for the above mentioned Ekman transports, and can thus be indirectly important for the ML-salinity in the NwAC.

Some of the weaker summer minima at OWSM have developed under southerly winds and must be attributed to other processes than direct westward Ekman transport. Additional processes that can influence the ML-salinity at OWSM are entrainment from below (of AW in summer and autumn, and perhaps from intermediate waters in winter) and horizontal advection and diffusion from the Arctic Water to the west.

6.4 Oxygen

6.4.1 Spatial and seasonal differences in the Norwegian Sea

The winter field of ML-oxygen (Figure 5d) shows that those parts of the Norwegian Sea that are governed by the warm AW have the lowest O_{ML} concentrations, with increasing values along the path of the NwAC and away from the axis of the flow. In contrast, the much colder Arctic waters to the west have significantly higher concentrations. This spatial resemblance between the winter fields of temperature and oxygen (Figures 5b and d) is expected, since with negligible biological activity during this time of the year the amount of oxygen that can be contained within the mixed layer is governed by the solubility concentration (mainly temperature dependent). As a result of heat loss from the AW to the atmosphere the solubility of oxygen increases during the northward flow of the NwAC, and the water is able to take up more oxygen from the atmosphere than further south. Mixing with adjacent water masses along the flow path, may, of course, increase the oxygen concentration of the AW. The effect of such mixing will be a reduction in the potential uptake of atmospheric

oxygen caused by the heat loss.

In summer the distribution of oxygen (Figure 5h) is in general more complex than during winter owing to in situ production of oxygen through biological activity, which counteracts the effect heating has upon the solubility concentration. Despite this, there is still a good spatial resemblance with the summer temperature field (Figure 5f), indicating that the solubility concentration has the governing effect on the oxygen content of the ML also during summer, with the oxygen produced escaping relatively quickly to the atmosphere. The oxygen field for the summer season shows nearly the same O_{ML} values as the winter field (Figure 5d). At OWSM for instance, both the mean winter and summer concentration are about 300 μmol L^{-1}. The reason for the lack of seasonal difference in the oxygen concentration fields seen in Figures 5d and h is that, in contrast to the MLD, O_{ML} has both its maximum and minimum value in the period chosen for the summer season (Jun–Sept, see Section 5.2), resulting in a mean value similar to the winter mean.

6.4.2 Mean annual cycle at OWSM

A clear annual cycle of oxygen does indeed exist in the upper parts of the Norwegian Sea as can be seen in Figure 6d. The figure shows that the mean annual oxygen cycle at OWSM has an amplitude of about 30 μmol L^{-1}. This is the same amplitude as the saturation concentration has when calculated from the annual temperature and salinity cycle. For the months September to March there is an increase in oxygen with decreasing temperatures. With increasing temperatures from April, a corresponding decrease in oxygen would have started was it not for the fact that primary production in this area starts in April–May and reaches its peak around June (Falck and Gade, 1999). A further increase in oxygen is therefore seen during the first months of spring. The increase in temperature during summer has its effects though, and although oxygen is still produced, the O_{ML} values are rapidly decreasing during the summer months, indicating that excess oxygen is released to the atmosphere. From September, one month after the peak in temperature, the O_{ML} steadily increases again with decreasing temperature.

In Figure 9c the hysteresis curves for both the oxygen concentration and the saturation concentration are shown, the latter calculated from monthly mean temperature and salinity values. This gives a good picture of how the oxygen concentration in the ML at OWSM deviates from what would be expected in a water parcel with no biological activity and with instant exchange of oxygen with the atmosphere after a given change in saturation concentration (i.e. temperature and/or salinity change). Starting in the upper left part of the figure, the oxygen hysteresis curve crosses the hysteresis curve of the saturation concentration between September and October and the water in the mixed layer changes from being oversaturated with respect to oxygen to becoming undersaturated. From this time on, the net flux of oxygen across the air–sea interface will be directed into the ocean. The difference between the saturation concentration and the oxygen concentration increases until January, indicating that the flux of oxygen to the surface water does not increase the oxygen concentration in the water fast enough to keep up with the increase in saturation concentration provided for by the change in temperature. During the winter months January–March the temperature change is small, but even so, the uptake of oxygen from the atmosphere does not lead to saturation concentrations. The reason for this is probably that the uptake of oxygen from the atmosphere has to be evenly distributed over a 300 m water column, and to raise the oxygen concentration in such a thick water column takes more time than is available before the change in season. Between April and May the water in the ML changes from being undersaturated to oversaturated with respect to oxygen. This change is caused by the combined effect of increasing temperatures in the mixed layer and the onstart of the biological season. The larger deviation of the ML-oxygen from the saturation concentration in June–July is due to a combination of high primary production, a respective slower exchange with the atmosphere, and a strongly stratified shallow ML inhibiting vertical transport of oxygen to the waters below.

The oxygen content in the upper 300 m at OWSM (Figure 7c, g) is very homogeneously distributed throughout the mixed layer from January to April. In the latter month a very small increase can be seen at the surface indicating the onset of primary production. Highest surface concentrations are seen in May with a mean concentration of 317 μmol L^{-1}, then the concentration steadily decreases until September, reaching a lowest mean value of 282 μmol L^{-1}. Below the summer mixed layer a relative maximum in oxygen concentration can be seen at about 25 m for the months July and August. This feature has also been seen elsewhere (Reid, 1962; Shulenberger and Reid, 1981), and is probably caused by oxygen produced below the shallow summer mixed layer, or is a remnant of the somewhat deeper May/June mixed layer, having no possibility to escape to the atmosphere due to the strong stratification above. A subsurface minimum at and below 50 m is also developing during summer due to remineralization of organic matter, while during the period of mixed layer deepening this minimum is gradually being mixed into the mixed layer and has disappeared by January.

The profiles of mean percent oxygen saturation (Figure 7d,h) show that the summer oversaturation is confined to the upper 25–50 m. Below 50 m the decrease in percent oxygen saturation from June to September/October (compared to the January–March profiles) is mainly due to consumption of oxygen by decomposition of organic matter. During the deepening phase of the mixed layer this low-oxygenated water is being entrained into the ML. The depth of the interface between the well-mixed surface layer and the low percent oxygen saturation layer gradually increases during the autumn following the changes in MLD. The mean percent oxygen saturation in the ML stays at a nearly constant value from November (98%) to March (98.5%). To maintain such a constant value there must be an input of oxygen to the ML during this period which balances the deficit in oxygen caused by the entrained low oxygen waters and the additional oxygen needed to keep the percent oxygen saturation at a constant value as the saturation concentration in the ML increases. The main source for this input has to be the atmosphere, estimations of oxygen fluxes for OWSM (Falck and Gade, 1999) show a considerable uptake of oxygen from the atmosphere during winter. Just below the MLD the mean percent saturation drops to about 95%.

6.4.3 The time series at OWSM

Unfortunately the oxygen time series (Figures 14 and 15) have more gaps than the time series of temperature and salinity. Due to the restricted amount of oxygen measurements (once a week) there are also more months that do not have a proper mean O_{ML} value compared to temperature and salinity. Since the monthly mean values are based on 1 to 5 O_{ML} values for each month, some of the monthly mean values presented here are not really representative for the whole month but only for shorter periods (i.e. one to two weeks). This must be kept in mind when analysing the time series.

Interannual variability is seen both in the spring peak values and in the late summer minimum (Figure 14). The high spring peaks in '75 (323 μmol L^{-1}) and '93 (342 μmol L^{-1}) are only based on measurements from one single station. The other years with maximum values above 320 μmol L^{-1} ('53, '63, '81, '92, and '94) are the mean of 2 to 4 O_{ML} values. The high peak in '92 is the mean of O_{ML} values from the two first weeks of June. During these weeks the measured oxygen concentration in the upper 10 m was high, 346.6 and 337.7 μmol L^{-1} respectively, and corresponding percent saturation were 125.8 and 128.9, the two highest percent oxygen saturation values for the whole period. Weather conditions at OWSM in early June '92 deviated substantially from other years between '80 and '95 (Gislefoss, Nydal, Slagstad, Sonninen, and Holmén, 1998) in being unusually calm and sunny. The strong heat input and anomalously warm mixed layer for this month (warmest June in the whole time series) are also seen in the time series of monthly mean heat input and ML-temperatures (Figure 10). Such weather conditions would minimize the air–sea exchange and most of the oxygen would be retained in the mixed layer. If the period coincided with the height of the spring bloom the resulting oxygen content in the upper layer could be high. In both '92 and '93 the mean ML in May was rather deep (196 and 162 m respectively) in contrast to the very shallow mean MLD values for June these years (18 and 23 m). These deep mixed layers suggest that the spring bloom probably did not start before June. The highest oxygen concentration measured in the upper 10 m, on the other hand, is found for June '95 with 357 μmol L^{-1} and a percent oxygen saturation of 125, whereas the monthly mean values (based on four values) are only 317 μmol L^{-1} and 110%, respectively. There is generally a rapid decrease in the surface concentrations (Figure 7g) after the shallow summer mixed layer ($\sim$20 m) has been established. It is therefore reasonable to assume that if there had been oxygen measurements for every week in June '92 and '93, the monthly mean value would have been considerably lower as is the case for '95. Furthermore, given the anomalously strong monthly mean wind mixing for June '92 shown in Figure 8, the last half of this month must have experienced high wind speeds and increased outgassing.

Of the mentioned years with higher than normal spring peaks, '75, '81, and '95 are from May and the other four from June. For the whole time series the maximum O_{ML} values are found in May for half the number of years and in June for the other half. This is also indicated in Figure 6d where means of the O_{ML} values for May and June are equal. Falck and Gade (1999) found that the mean biological net production at OWSM, based on an oxygen budget, was highest and more or less equal for the months of May and June. This indicates that the timing of the spring bloom varies from year to year, depending on hydrographical and meteorological conditions, with the initiation of the bloom probably being mainly dependent on physical stabilization of the upper water column. In years with an early stabilization, the spring bloom starts earlier giving highest O_{ML} values for May, whereas a later stabilization results in highest O_{ML} values in June. Furthermore, May is the only month of the year where a clear negative correlation was found between the depth of the mixed layer and the O_{ML} values (not shown). The lowest mean O_{ML} value in the time series is found for August of '61 and '88 with a mean O_{ML} value of 272 μmol L^{-1} (based on three O_{ML} values for both years). For the whole time

series, the lowest mean O_{ML} value occurs in September, except for the years '61, '71, '76, '85, '86, '88, and '91 where it occurs in August.

The time series of monthly mean $O^{\%}_{ML}$ (percent oxygen saturation; Figure 15) shows a yearly variation from about 98% in winter to about 110% in summer with interannual variability especially in summer. The month with highest $O^{\%}_{ML}$ value during one year is generally June or July, with only a few exceptions. Overall the five months May to September have $O^{\%}_{ML}$ values above 100%, but some years have 3, 4, or 6 months where the mixed layer is oversaturated. For most of the years May is the first month with oversaturated mixed layer values, but for a few years it already occurred in April and in a few others not until June. In autumn, the last month with values above 100% is normally September, but in some of the years this has occurred in August or October, and once in November. The $O^{\%}_{ML}$ values above 110% are mainly from June months that have MLD shallower than 25 m.

For both the O_{ML} and $O^{\%}_{ML}$ values it is difficult to find an explicit cause for the interannual variability seen in summer from variations in physical properties. Regressing the time series of O_{ML} and $O^{\%}_{ML}$ against the other time series of mixed layer properties does not give any significant correlation, but performing the same regressions for individual calendar months gave some correlation (r>0.5) with one or more of the other ML-properties in a few cases, but most months do not show any correlation at all (not shown). Interannual variability in both the strength of the biological production and the duration of the blooming season are therefore the most plausible causes for the summer oxygen variability. Variations in the meteorological forcing, governing the conditions at the surface and hence the resulting air–sea gas exchange, probably also plays a major role in this aspect.

7 Summary and conclusions

The spatial variability of the mixed layer properties in the Norwegian Sea clearly reflects the different water masses and circulation patterns representative of the region. The area studied is dominated by the inflow of warm and saline AW, which contrasts the neighbouring coastal and Arctic waters. For most of the AW domain and in the time series at OWSM, the winter MLD follows the depth of S=35, indicating that the mixing generally reaches through the whole column of AW in this season. Along the path of the NwAC in the southern Norwegian Sea, the mean winter MLD is around 300 m and slanting towards the surface in the central Norwegian Basin. The MLD increases over the Vøring Plateau, and noticeably when the flow enters the Lofoten Basin where a mean wintertime mixing depth of ∼600 m is reached. Since the mean depth of S=35 in the Lofoten Basin reaches ∼800 m, this indicates a lesser degree of through mixing of the whole AW column in this basin than further south. The relative importance of the dynamics of the NwAC and the atmospherically forced mixing for determining the winter MLD and depth of the AW remains undetermined. However, localisation of deep mixed layers over the topographical features rather than in accordance with the field of atmospheric buoyancy flux indicates that the general circulation is a governing factor for the common depth of AW and wintertime mixed layer, through both increased residence times in the convective areas and dynamic control of the lower boundary of the AW.

A significant feature during summer is an area of rather shallow mixed layer with low salinity and strong stability across the NwAC at around 64–66°N. Furthermore, in some years a clear freshening takes place during summer at OWSM. This freshening is found to occur mainly in months when the influence of northerly winds is strong, which gives an Ekman transport of coastal water into the Atlantic domain. This advection is facilitated by the shallow summer mixed layer in which the freshwater signal can be advected farther offshore than in winter when mixing is deep. Precipitation cannot be the cause of these freshening events since they always coincide with periods of strong evaporation. In fact evaporation is dominating at OWSM throughout the year, while precipitation dominates over the neighbouring waters. Thus any influence of precipitation on the AW can mainly be achieved indirectly via lateral advection.

On its way northward over the 12 degrees of latitude studied, the AW is on average shown to cool from 8 to 5°C, reduce its salinity from 35.25 to 35.05 (i.e. increase its density by 0.2 kg m^{-3}), and increase its oxygen concentration from 290 to 310 μmol L^{-1}. The cooling and consequent oxygen increase is due to heat loss to the atmosphere during winter, while vertical mixing in autumn of the fresh coastal influenced surface water is considered the main mechanism for freshening of the northward flowing AW.

At OWSM the different properties of the mixed layer follow a mean annual cycle but with clear variations from year to year. The vertical gradients that have developed during spring and summer are efficiently mixed out during autumn. The annual variability of the properties is confined to the upper 300 m. Maximum temperatures in the mixed layer are between 11 and 13°C and usually reached in August. The accumulated heat input during

spring and summer is the controlling factor of the interannual variability in maximum summer mixed layer temperature. The rate of autumn deepening is strongly determined by wind mixing and convective forcing from the atmosphere. The minimum in temperature is about 6°C and usually reached in March. The core of the NwAC, which is detached from the mixed layer during summer, has a salinity maximum in July–September and minimum in December, while the temperature cycle at this depth lag salinity by three months. The downward mixing of the surface freshwater and heat from the summer layer and the winter cooling of the NwAC are most likely the underlying mechanisms behind the delayed seasonality of the northward flowing AW.

Mixed layer oxygen shows highest values in May–June (310 μmol L^{-1}) and lowest in August-September (280 μmol L^{-1}). Interannual variability is seen both in the spring peak values (300–320 μmol L^{-1}) and in the late summer minima (270–290 μmol L^{-1}). The oxygen concentration in the mixed layer at OWSM is governed by the temperature cycle. Any deviation from the temperature dependent saturation concentration is caused by the relatively slow rate of exchange with the atmosphere giving time for an excess of oxygen to develop in the mixed layer at times of primary production and a deficit during winter due to entrainment of water with lower oxygen content during the deepening phase of the mixed layer. Even though the increase in MLD and the temperature changes are very small from January to March, the percent oxygen saturation stays nearly constant around 98% during these months, indicating that the time needed for the atmospheric flux to raise the oxygen concentration to saturation levels is not sufficient before the change in season.

It is clear from this work that in an area like the Norwegian Sea, with strong spatial variations in hydrography and existence of prominent currents, interpretation of mixed layer properties solely from ocean station time series and 1D models can only be viewed as a first order approach. The lateral exchanges of water masses between the coastal-, Atlantic-, and Arctic Waters in the Norwegian Sea needs to be quantified and their forcing mechanisms studied more closely. This is important since the modification of Atlantic Water through lateral advection and the distribution of AW between the ocean interior and the shelf areas both have implications for the marine climate and deep water formation processes in the Nordic Seas and Arctic.

8 Acknowledgments

We are grateful to Alexander Korablev for the hydrographic database compiled at AARI and NERSC. Knut Iden at met.no is thanked for meteorological station data. The NCEP/NCAR Reanalysis data is provided by the NOAA-CIRES Climate Diagnostics Center, Boulder, Colorado, USA, from their Web site at http://www.cdc.noaa.gov/. Many thanks to Svein Østerhus for help with the OWSM data and to Tore Furevik and Asgeir Sorteberg for help with the reanalysis data. The authors also want to thank Ken Drinkwater and two anonymous reviewers who provided constructive comments that greatly improved an earlier version of the manuscript. This work was initiated when one of the authors (E. Falck) was working at the Department of Analytical and Marine Chemistry, Göteborg University, Sweden. J.E.Ø. Nilsen has been supported by the Research Council of Norway through the RegClim project, and the G.C. Rieber Foundations. This is publication number A 127 from the Bjerknes Centre for Climate Research.

References

Alekseev, G. V., Johannessen, O. M., Korablev, A. A., Ivanov, V. V., & Kovalevski, D. V. (2001). Interannual variability of water mass in the Greenland Sea and the adjacent areas. *Polar Research*, 20(2), 201–208.

Belkin, I. M. (2004). Propagation of the "Great Salinity Anomaly" of the 1990's around the northern North Atlantic. *Geophysical Research Letters*, 31, L08306, doi:10.1029/2003GL019334.

Belkin, I. M., Levitus, S., Antonov, J., & Malmberg, S.-A. (1998). "Great Salinity Anomalies" in the North Atlantic. *Progress in Oceanography*, 41(1), 1–68.

Blindheim, J. (1990). Arctic Intermediate Water in the Norwegian Sea. *Deep–Sea Research*, 37(9), 1475–1489.

Blindheim, J. (1993). Seasonal variations in the Atlantic inflow to the Nordic Seas. *ICES CM 1993/C*, 39.

Blindheim, J., Borovkov, V., Hansen, B., Malmberg, S. A., Turrell, W. R., & Østerhus, S. (2000). Upper layer cooling and freshening in the Norwegian Seas in relation to atmospheric forcing. *Deep–Sea Research I*, 47(4), 655–680.

Blindheim, J. & Østerhus, S. (2005). The Nordic Seas, main oceanographic features. In H. Drange, T. Dokken, T. Furevik, R. Gerdes, & W. Berger, (Eds.), *The Nordic Seas: An Integrated Perspective*, volume 158 of *Geophysical Monograph Series*. American Geophysical Union, Washington DC, pp. 11–38.

Bøyum, G. (1966). The energy exchange between sea and atmosphere at Ocean Station M, I and A. *Geophysica Norvegica*, 26(7).

Brainerd, K. E. & Gregg, M. C. (1995). Surface mixed and mixing layer depths. *Deep–Sea Research I*, 42(9), 1521–1543.

Bunker, A. F. (1976). Computations of surface energy flux and annual air-sea interaction cycles of the North Atlantic Ocean. *Monthly Weather Review*, 104(9), 1122–1140.

Colt, J. (1984). *Computation of Dissolved Gas Concentrations in Water as Functions of Temperature, Salinity, and Pressure*, volume 14 of *American Fisheries Society Special Publications*. American Fisheries Society, Bethesda, MD, 154 pp.

Dickson, R. (1972). Variability and continuity within the Atlantic Current of the Norwegian Sea. *Rapp. Procès-Verbaux Réunions. Conseil International l'Exploration de la Mer*, 162, 167–183.

Dickson, R. R., Meincke, J., Malmberg, S.-A., & Lee, A. J. (1988). The "Great Salinity Anomaly" in the northern North Atlantic 1968–1982. *Progress in Oceanography*, 20(2), 103–151.

Falck, E. & Gade, H. G. (1999). Net community production and oxygen fluxes in the Nordic Seas based on O_2 budget calculations. *Global Biogeochemical Cycles*, 13(4), 1117–1126.

Fofonoff, P. & Millard, Jr, R. (1983). *Unesco 1983. Algorithms for Computation of Fundamental Properties of Seawater*. Technical Report 44, UNESCO technical papers in marine science, 53 pp.

Furevik, T., Bentsen, M., Drange, H., Johannessen, J. A., & Korablev, A. (2002). Temporal and spatial variability of the sea surface salinity in the Nordic Seas. *Journal of Geophysical Research*, 107(C12), 8009, doi:10.1029/2001JC001118.

Gade, H. (1986). Features of fjord and ocean interaction. In B. G. Hurdle, (Ed.), *The Nordic Seas*, chapter 7. Springer Verlag, pp. 185–189.

Gammelsrød, T. & Holm, A. (1984). Variations of temperature and saltinity at Station M (66°N 02°E) since 1948. *Rapp. Procès-Verbaux Réunions. Conseil International l'Exploration de la Mer*, 185, 188–200.

Gammelsrød, T., Østerhus, S., & Godøy, Ø. (1992). Decadal variations of ocean climate in the Norwegian Sea observed at Ocean Station "Mike" (66°N 2°E). In R. Dickson, P. Mälkki, R. S. G. Radach, & M. Sissenwine, (Eds.), *Hydrobiological Variability in the ICES Area, 1980-89*, volume 195 of *ICES Marine Science Symposia*, ICES, pp. 68–75.

Gislefoss, J. S., Nydal, R., Slagstad, D., Sonninen, E., & Holmén, K. (1998). Carbon time series in the Norwegian Sea. *Deep–Sea Research I*, 45(2–3), 433–460.

Glover, D. M. & Brewer, P. G. (1988). Estimates of wintertime mixed layer nutrient concentrations in the North Atlantic. *Deep–Sea Research*, 35(9), 1525–1546.

Hansen, B. & Østerhus, S. (2000). North Atlantic–Nordic Seas exchanges. *Progress in Oceanography*, 45(2), 109–208.

Helland, P. (1963). Temperature and salinity variations in the upper layers at Ocean Weather Station M (66°N, 2°E). *Universitetet i Bergen Årbok Matematisk–Naturvitenskapelig Rekke*, 16, 26 pp.

Helland-Hansen, B. & Nansen, F. (1909). The Norwegian Sea: Its physical oceanography. In J. Hjort, (Ed.), *Rep. Norw. Fish. Mar. Inv.*, volume II. The Royal Department of Trade, Navigation and Industries, Oslo, Norway, 390 pp.

Ivanov, V. & Korablev, A. (1995a). Formation and regeneration of the pycnocline lens in the Norwegian Sea. *Russian Meteorology and Hydrology*, 9, 62–69.

Ivanov, V. & Korablev, A. (1995b). Interpycnocline lens dynamics in the Norwegian Sea. *Russian Meteorology and Hydrology*, 10, 32–37.

Johannessen, J., Svendsen, E., Sandven, S., Johannssen, O., & Lygre, K. (1989). Three dimensional structure of meso scale eddies in the Norwegian Coastal Current. *Journal of Physical Oceanography*, 19, 3–19.

Johannessen, J. A. & Gade, H. G. (1984). A case study of the variations in the upper ocean at Ocean Weather Ship Mike (66°N, 2°E) in the Norwegian Sea. *Geophysica Norvegica*, 32(5), 165–175.

Johannessen, O. M., Alekseev, G., Ivanov, V., Korablev, A., Kovalevsky, D., Myakoshim, O., et al. (2000). *Detection and Modelling of Greenhouse Warming in the Arctic and Sub-Arctic. Oceanographic Data Analysis: Greenland Sea.* Technical Report Task 3, INTAS 97-1277, Nansen Environmental and Remote Sensing Center/Arctic and Antarctic Research Institute, Thormøhlensgt.47, 5006 Bergen, Norway.

Kalnay, E., Kanamitsu, M., Kistler, R., Collins, W., Deaven, D., Gandin, L., et al. (1996). The NCEP/NCAR 40-year reanalysis project. *Bulletin of the American Meteorological Society*, 77(3), 437–471.

Kantha, L. H. & Clayson, C. A. (2000). *Small Scale Processes in Geophysical Fluid Flows*, volume 67 of *International Geophysics Series*. Academic Press, San Diego, 888 pp.

Kara, A. B., Rochford, P. A., & Hurlburt, H. E. (2000a). Mixed layer depth variability and barrier layer formation over the North Pacific Ocean. *Journal of Geophysical Research*, 105(C7), 16 783–16 801.

Kara, A. B., Rochford, P. A., & Hurlburt, H. E. (2000b). An optimal definition for ocean mixed layer depth. *Journal of Geophysical Research*, 105(C7), 16 803–16 821.

Kara, A. B., Rochford, P. A., & Hurlburt, H. E. (2003). Mixed layer depth variability over the global ocean. *Journal of Geophysical Research*, 108(C3), 3079, doi:10.1029/2000JC000736.

Lalli, C. M. & Parsons, T. R. (1997). *Biological Oceanography: An Introduction.* Butterworth-Heinemann, Oxford, 301 pp.

Leinebø, R. (1991). Oxygen variation in the Arctic Intermedite Water at Ocean Weather Station Mike (66°N 2°E). *ICES CM 1991/C*, 6.

Lukas, R. & Lindström, E. (1991). The mixed layer of the western equatorial Pacific-Ocean. *Journal of Geophysical Research*, 96, Suppl. S, 3343–3357.

Marshall, J. & Schott, F. (1999). Open-ocean convection: Observations, theory, and models. *Reviews of Geophysics*, 37(1), 1–64.

Mauritzen, C. (1996a). Production of dense overflow waters feeding the North Atlantic across the Greenland–Scotland Ridge. Part 1: Evidence for a revised circulation scheme. *Deep–Sea Research I*, 43(6), 769–806.

Mauritzen, C. (1996b). Production of dense overflow waters feeding the North Atlantic across the Greenland–Scotland Ridge. Part 2: An inverse model. *Deep–Sea Research I*, 43(6), 807–835.

McDougall, T. J. (1987). Neutral surfaces. *Journal of Physical Oceanography*, 17, 1950–1964.

Mikki, S. (1998). *Quality Control of Salinity Data from Station M.* Report 74, Geophysical Institute, University of Bergen, Allégt.70, 5007 Bergen, Norway. Unpublished.

Mork, K. A. (2006). Decadal hydrographic variability in the central Norwegian Sea. *Journal of Geophysical Research.* Pers. Comm.

Mork, K. A. & Blindheim, J. (2000). Variation in the Atlantic Inflow to the Nordic Seas, 1955–1996. *Deep–Sea Research I*, 47(6), 1035–1057.

Mosby, H. (1950). Recherches océanographiques dans la mer de Norwège a la Station Météorologique M. *Cahiers du Centre de Recherches et D'etudes Océanographiques*, 1, 1–7.

Mosby, H. (1959). Deep water in the Norwegian Sea. *Geophysica Norvegica*, 21(3), 62 pp.

Mosby, H. (1962). Water, salt, and heat balance of the North Polar Sea and of the Norwegian Sea. *Geophysica Norvegica*, 24(11), 289–313.

Mosby, H. (1970). Atlantic Water in the Norwegian Sea. *Geophysica Norvegica*, 28(1), 60 pp.

Mosby, H. (1974). Diffusion and bottom water in the Norwegian Sea. In C. international sur les processus de formation des eaux océaniques profondes (1972)., (Ed.), *Processus de formation des eaux océaniques profondes, en particulier en Méditerranée occidentale : Paris, 4–7 Octobre 1972. Laboratoire d'océanographie physique du muséum.*, Colloques internationaux du Centre national de la recherche scientifique ; no 215. C.N.R.S., Paris, pp. 59–74.

Niiler, P. P. & Kraus, E. B. (1977). One-dimensional models of the upper ocean. In E. B. Kraus, (Ed.), *Modelling and Prediction of the Upper Layers of the Ocean: Proceedings of a NATO Advanced Study Institute*, volume 1 of *Pergamon marine series*. Pergamon Press, Oxford. Proceedings of a NATO Advanced Study Institute, pp. 143-172.

Nilsen, F. (2004). Forcing of a two-layered water column over a sloping sea floor. *Journal of Physical Oceanography*, 35, 2659–2676.

Nilsen, J. E. Ø. (2003). *Aspects of the Atlantic Flow through the Norwegian Sea.* Dr. scient. thesis in physical oceanography, Geophysical Institute, University of Bergen, Allégt.70, 5007 Bergen, Norway. Reports in Meteorology and Oceanography, University of Bergen, Report No. 3-2003 (www.nersc.no/∼even/doc/thesis). Unpublished.

Nilsen, J. E. Ø. & Nilsen, F. (2003). The Atlantic Water flow along the Vøring Plateau: Detecting frontal structures in oceanic station time series. *Deep–Sea Research I.* Pers. Comm.

Orvik, K. A. & Niiler, P. (2002). Major pathways of Atlantic water in the northern North Atlantic and Nordic Seas towards arctic. *Geophysical Research Letters*, 29(19), 1896, doi:10.1029/2002GL015002.

Orvik, K. A., Skagseth, Ø., & Mork, M. (2001). Atlantic Inflow to the Nordic Seas. Current structure and volume fluxes from moored current meters, VM–ADCP and SeaSoar-CTD observations, 1995–1999. *Deep–Sea Research I*, 48(4), 937–957.

Østerhus, S. & Gammelsrød, T. (1999). The abyss of the Nordic Seas is warming. *Journal of Climate*, 12(11), 3297–3304.

Polovina, J. J., Mitchum, G. T., & Evans, G. T. (1995). Decadal and basin-scale variation in mixed layer depth and the impact on biological production in the Central and North Pacific, 1960–88. *Deep–Sea Research I*, 42(10), 1701–1716.

Poulain, P.-M., Warn-Varnas, A., & Niiler, P. (1996). Near surface circulation of the Nordic Seas as measured by lagrangian drifters. *Journal of Geophysical Research*, 101(C8), 18 237–18 258.

Read, J. & Pollard, R. (1992). Water Masses in the Region of the Iceland–Færoes Front. *Journal of Physical Oceanography*, 22(11), 1365–1378.

Redfield, A. C. (1948). The exchange of oxygen across the sea surface. *Journal of Marine Research*, 7(3), 347–361.

Reid, J. (1962). Distribution of dissolved oxygen in the summer thermocline. *Journal of Marine Research*, 20(2), 138–148.

Rey, F. (1981). The development of the spring phytoplankton outburst at selected sites off the Norwegian Coast. In R. Sætre & M. Mork, (Eds.), *The Norwegian Coastal Current*, volume 2. Geophysical Institute, University of Bergen, Bergen, pp. 649–680.

Rochford, P. A., Kara, A. B., Wallcraft, A. W., & Arnone, R. A. (2001). Importance of solar subsurface heating in ocean general circulation models. *Journal of Geophysical Research*, 106(C12), 30 923–30 938.

Russenes, E. (1957). *Overflatestrømmen på Værskipsstasjon M, 66° N, 2° E.* Master's thesis, Geophysical Institute, University of Bergen, Allégt.70, 5007 Bergen, Norway. Unpublished.

Sælen, O. H. (1963). Studies in the Norwegian Atlantic Current. Part II: Investigations during the years 1954-59 in an area west of Stad. *Geophysica Norvegica*, 23(6), 82 pp.

Sætre, R., Aure, J., & Ljøen, R. (1988). Wind effects on the lateral extent of the Norwegian Coastal Current. *Continental Shelf Research*, 8(3), 239–253.

Shulenberger, E. & Reid, J. L. (1981). The Pacific shallow oxygen maximum, deep chlorophyll maximum, and primary productivity, reconsidered. *Deep–Sea Research*, 28(9), 901–919.

Skjelvan, I., Falck, E., Anderson, L. G., & Rey, F. (2001). Oxygen fluxes in the Norwegian Atlantic Current. *Journal of Marine Chemistry*, 73(3–4), 291–303.

Smart, J. H. (1984). Spatial variability of major frontal systems in the North Atlantic-Norwegian Sea area: 1980–1981. *Journal of Physical Oceanography*, 14(1), 185–192.

Svendsen, E., Sætre, R., & Mork, M. (1991). Features of the northern North Sea circulation. *Continental Shelf Research*, 11(5), 493–508.

Taylor, A. H. & Stephens, J. A. (1980). Seasonal and year-to-year variations in surface salinity at the nine North Atlantic ocean weather stations. *Oceanologica Acta : Revue Européenne d'Océanologie*, 3(4), 421–430.

Weiss, R. F. (1970). The solubility of nitrogen, oxygen and argon in water and seawater. *Deep–Sea Research*, 17(4), 721–735.

Table 1: Overall estimated error for the mean values in the different fields in Figure 5. Worst cases are indicated in parenthesis. The error is calculated as $\sigma_m^2 \approx \sigma^2/(N-1)$, where N is number of data points in a bin.

		Winter		Summer	
σ_m(MLD)	[m]	25	(50[a])	3	(5[b])
$\sigma_m(T_{ML})$	[°C]	0.2		0.3	
$\sigma_m(S_{ML})$		0.01	(<0.08[c])	0.02	(0.1[c])
$\sigma_m(O_{ML})$	[μmol L^{-1}]	4		10	

[a]North of 70°N.
[b]In Lofoten Basin, 70°N.
[c]In coastal areas.

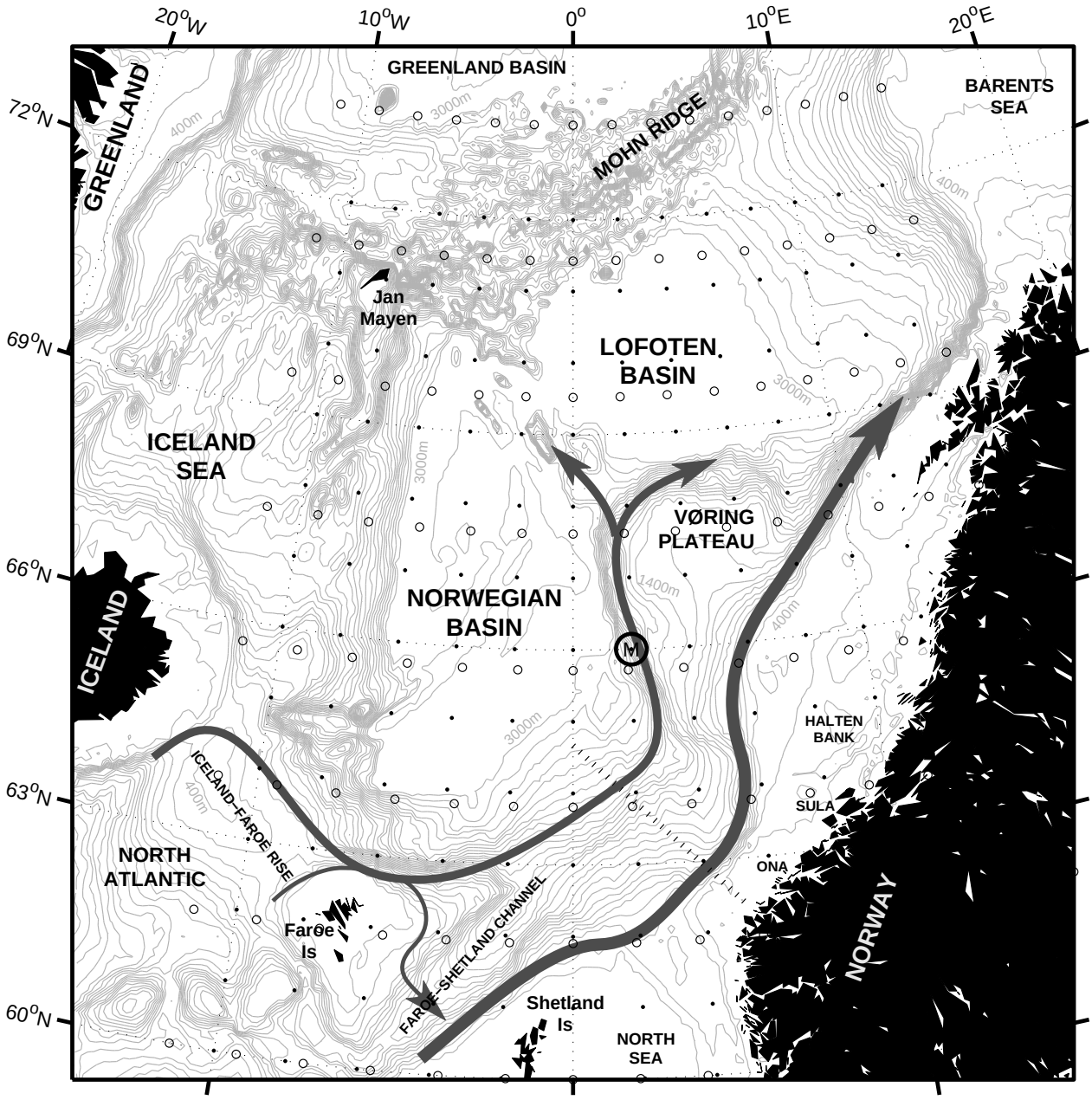

Figure 1: Bathymetry of the Norwegian Sea. Isobaths every 100 m from 200 to 3000 m, and at 3500 m. OWSM (circled M) is situated above the slope southwest of the Vøring Plateau in or near the topographically steered baroclinic western branch of the Norwegian Atlantic Current (NwAC; arrows). Open circles indicate positions of NCEP/NCAR atmospheric reanalysis data. Points indicate centers of the bins with hydrographic data from AARI. Dotted line south of OWSM indicates the Svinøy Section.

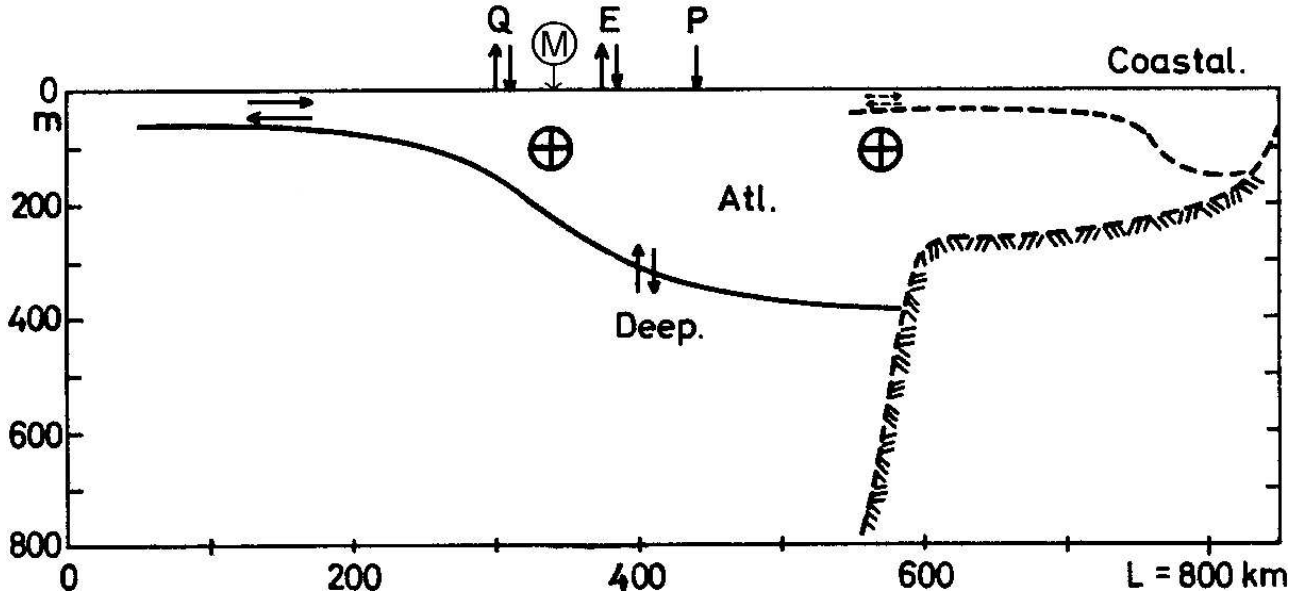

Figure 2: Conceptual cross section of the Norwegian Atlantic Current in the southern Norwegian Sea, with coastal-, Atlantic-, and deep water layering one another from east (right) to west (left) and top to bottom. From Mosby (1970), modified with indication of a two branch current and OWSM position.

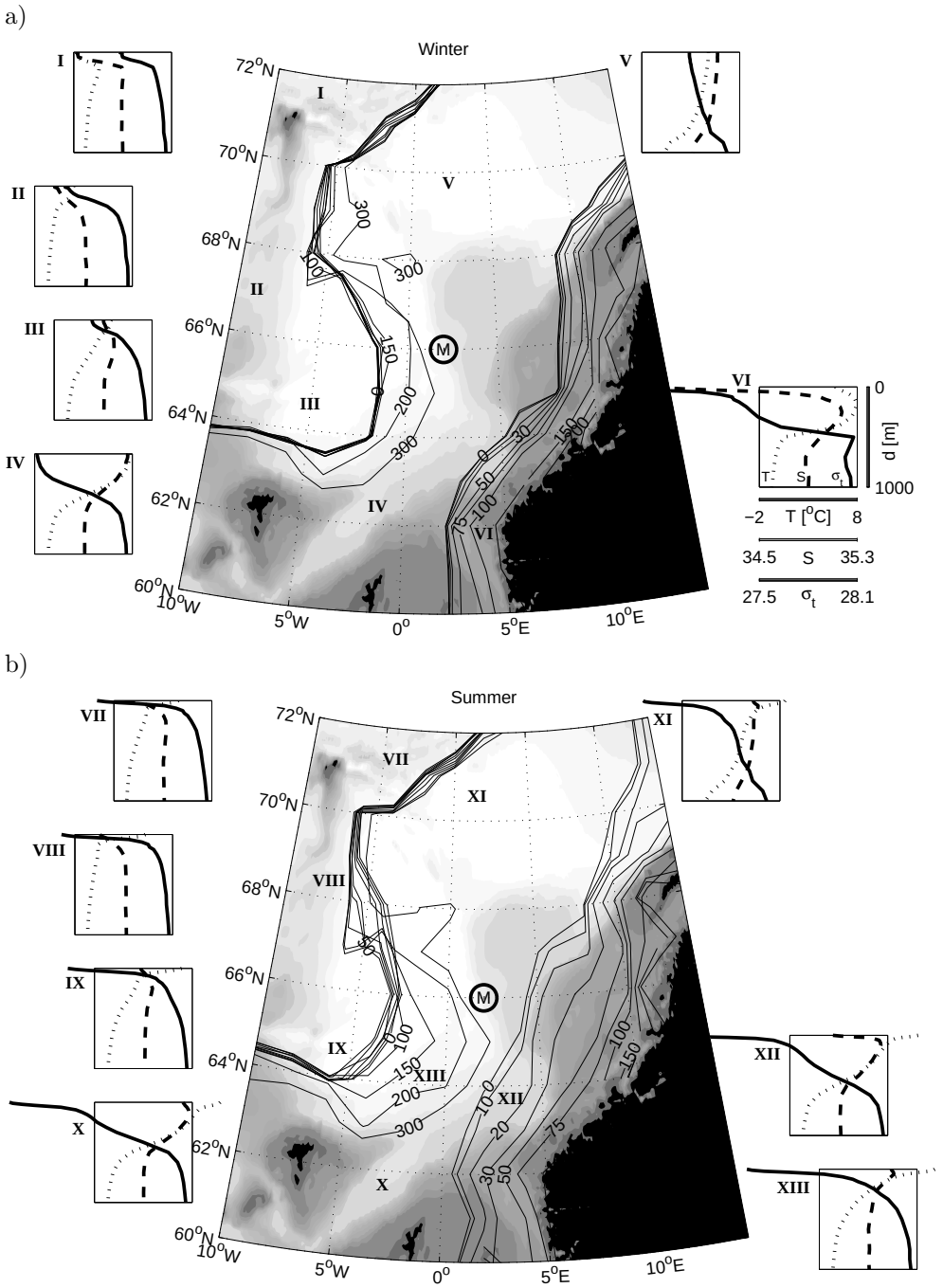

Figure 3: Depth contours of isohaline surfaces for salinity of 35, the traditional border between the AW and the surrounding waters, as mean fields from binned AARI hydrographic data for a) winter and b) summer. The eastern surface shows the top of the AW while the western surface shows the base of the AW. Background shading indicates bottom topography. The deeper part of the western isohaline surface (not shown) continues in toward the continental slope under the coastal waters. Roman numbers give positions for chosen average profiles of density (solid), salinity (dashed), and temperature (dotted) shown in the inlays. All inlays have the same axis limits as Inlay VI.

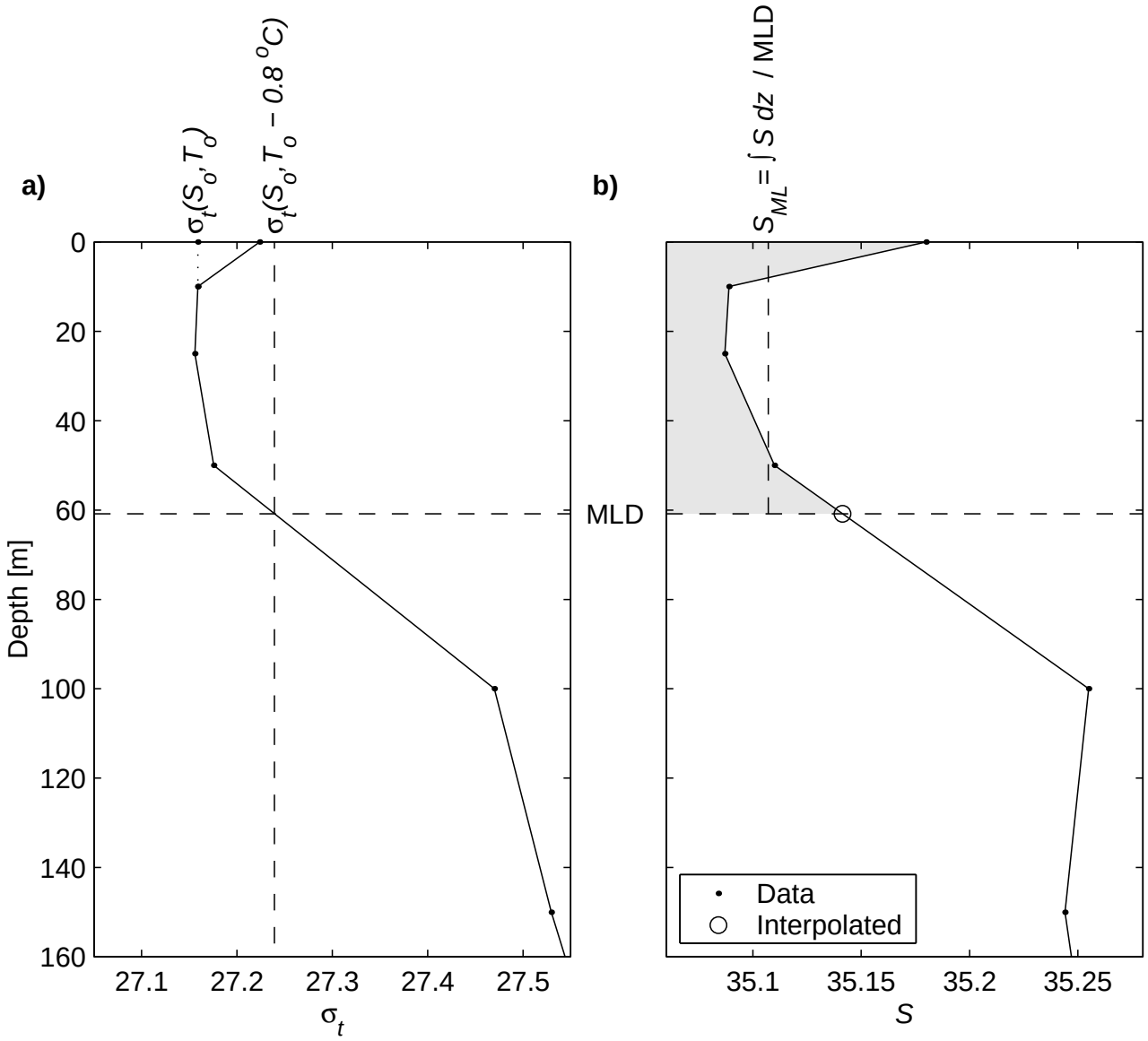

Figure 4: a) The method of finding MLD: An MLD-density is calculated from surface salinity (S_0) and temperature (T_0), subtracting 0.8°C from the latter. The corresponding MLD is found by linear interpolation in the density profile (dashed lines). The profile shown here is one of the cases with surface instability, where the first "stable" data point is used instead (dotted line). b) The integrated ML-property (here salinity) is found by trapezoidal integration between data points and the value at the base found by interpolation.

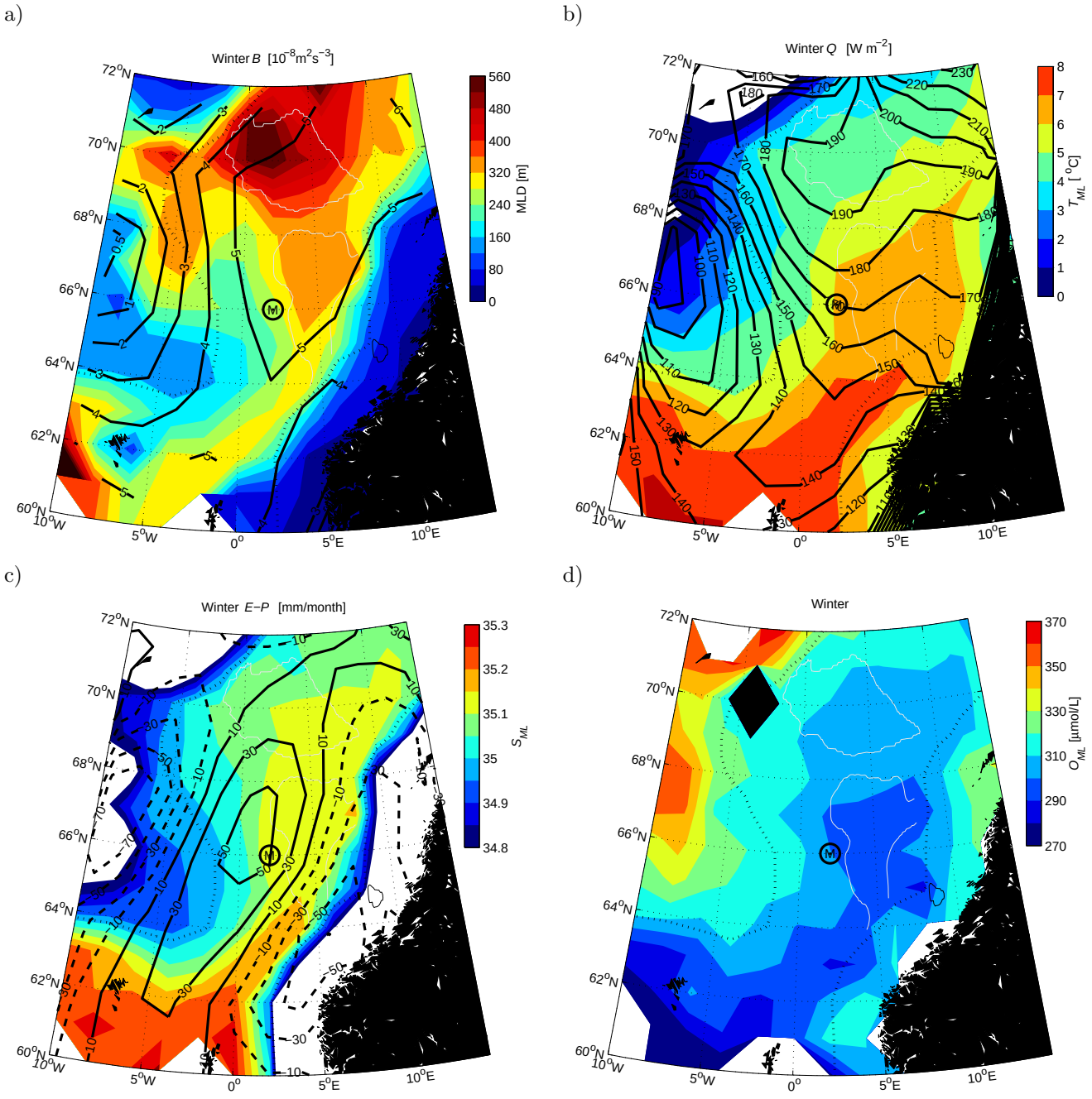

Figure 5: Mean fields for the winter (Dec–Apr; a–d) and summer (Jun–Sept; e–h) of a,e) mixed layer depth (colour) and buoyancy flux to the atmosphere (black contours), b,f) ML-temperature (colour) and heat flux to the atmosphere (black contours), c,g) ML-salinity (colour) and net freshwater fluxes to the atmosphere (black contours), and d,h) ML-oxygen. This is based on AARI-hydrography from the last 50 years, and reanalysis data. (Continued on next page)

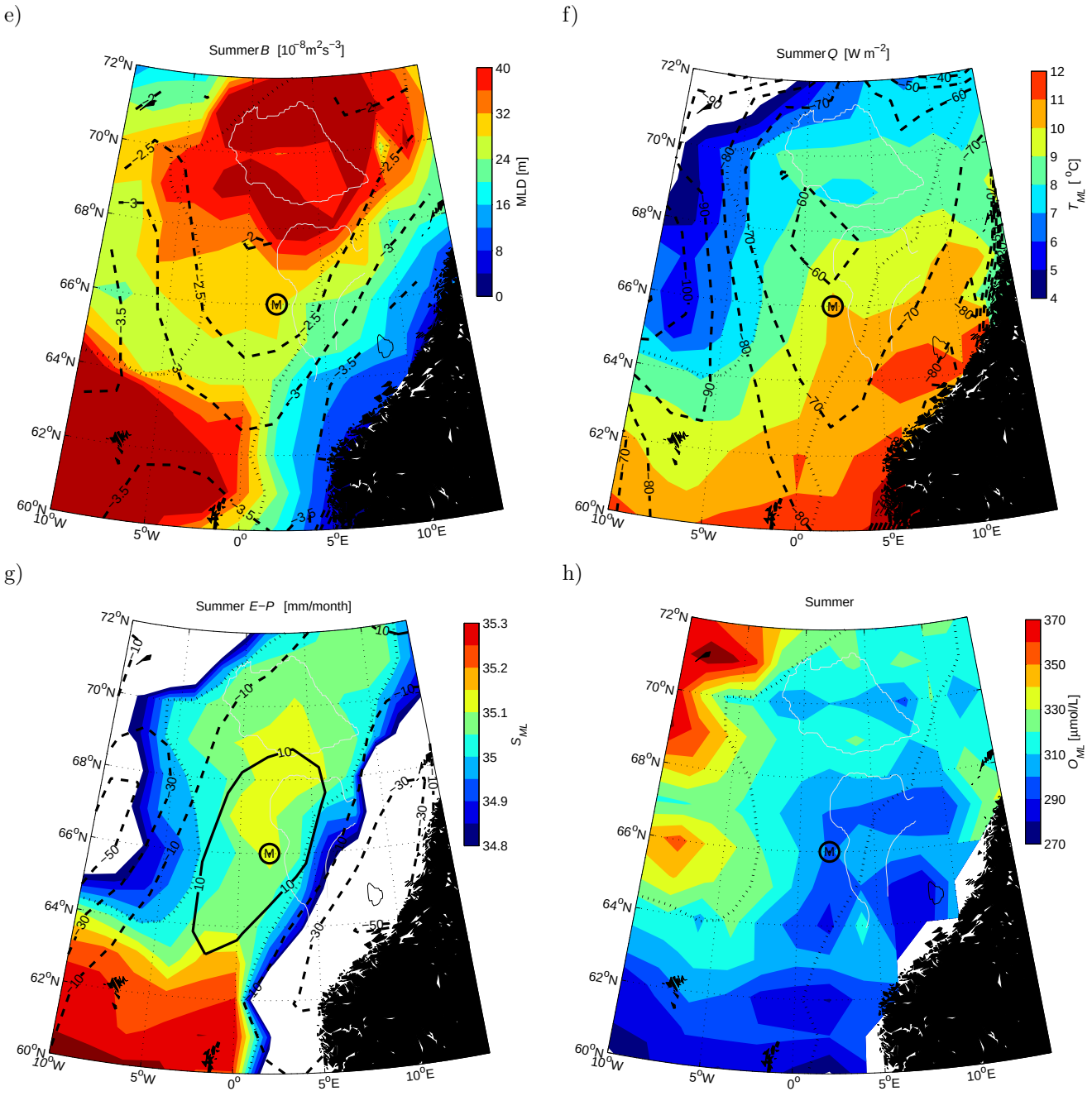

Figure 5: (continued) Full lines indicate positive atmospheric fluxes while dashed lines indicate negative. Atlantic Water is outlined by dotted S=35 surface isohalines. White contours are isobaths outlining (from top) the deep Lofoten basin (3100 m), the Vøring Plateau (1500 m) and the Norwegian Continental Shelf (500 m). The closed black isobath (200 m) near 8°E,65°N shows the Halten Bank. Circled M shows the position of OWSM.

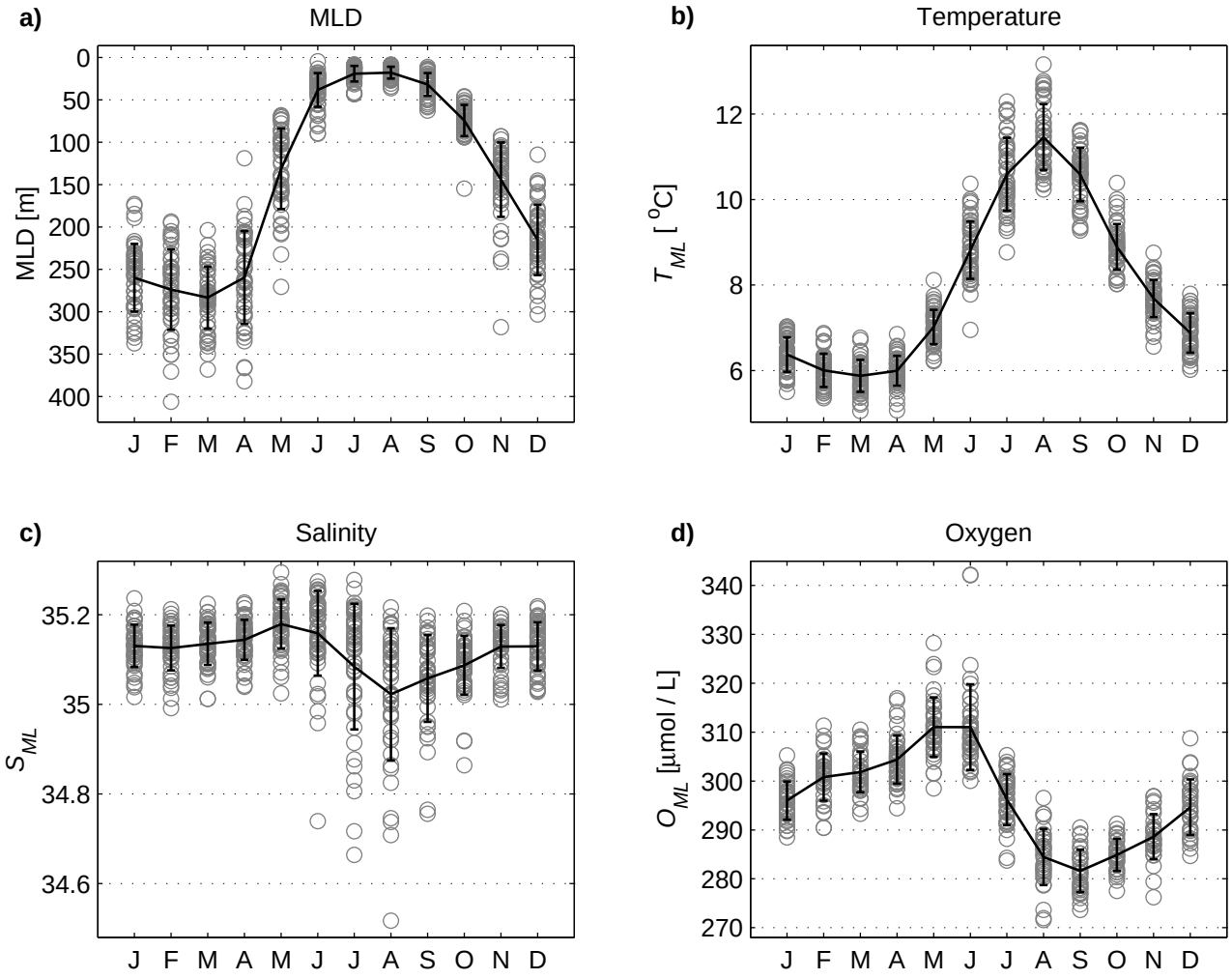

Figure 6: Monthly mean values of a) MLD, b) T_{ML}, c) S_{ML}, and d) O_{ML} from OWSM, by month of year (circles). The lines are drawn between means for each month and thus outline the empirical annual cycles. Error bars indicate one standard deviation.

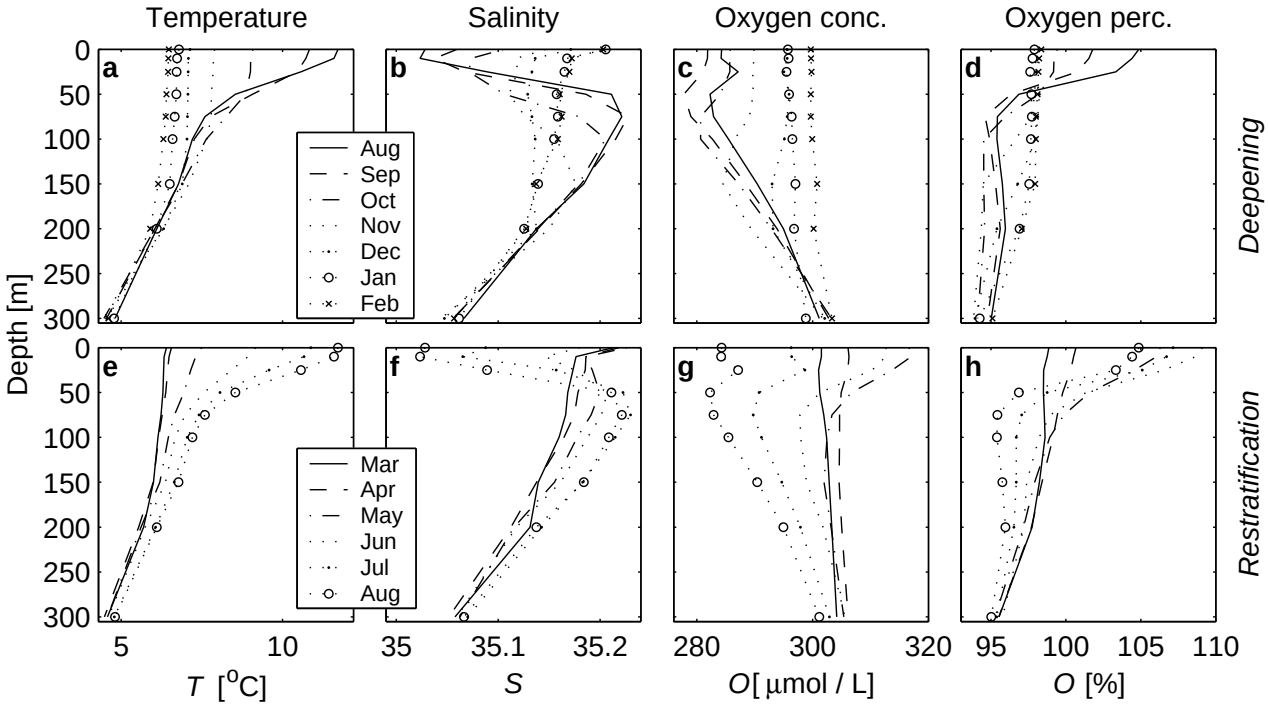

Figure 7: Monthly mean profiles showing the annual cycles of temperature (a, e), salinity (b, f), oxygen concentration (c, g), and oxygen saturation (d, h) in the upper 300 m at OWSM. The density follows closely the inverse of the temperature profile.

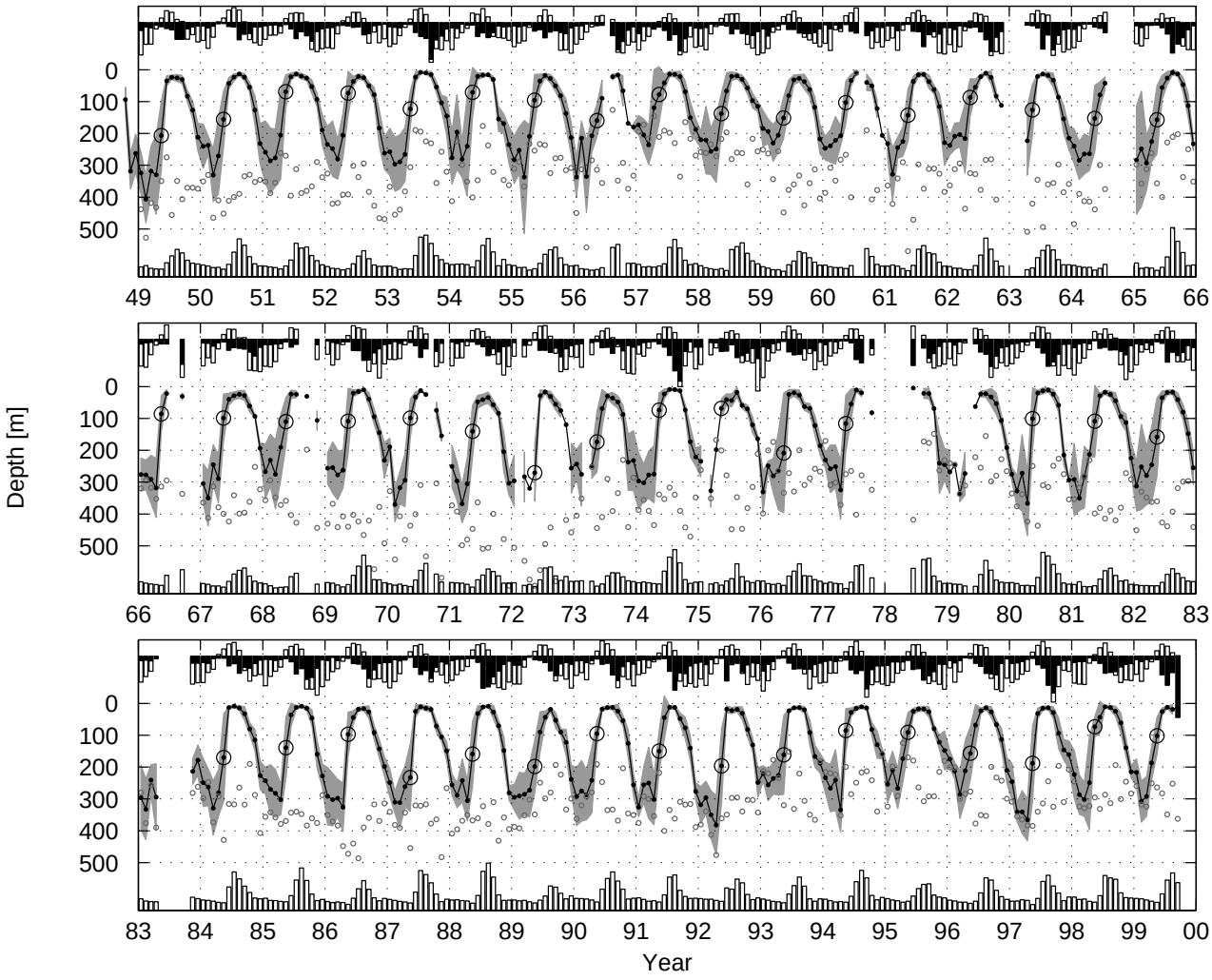

Figure 8: Monthly mean mixed layer depth at OWSM, for the whole period (black line with dots). The shaded area indicates an error estimate using plus/minus one standard deviation of the population in the month. Gaps in the shaded area indicate months with only one station, and thus no standard deviation available. May months are circled. Bar graphs above show relative contribution to entrainment velocity from wind stress (u_*^3 / MLD; filled bars) and buoyancy flux (B; open bars) from the nearest upstream reanalysis gridpoint (see Figure 1). Downward pointing bars are positive. Bars below indicate stability at base (Δb). Small (grey) circles indicate monthly mean depths of S=35.

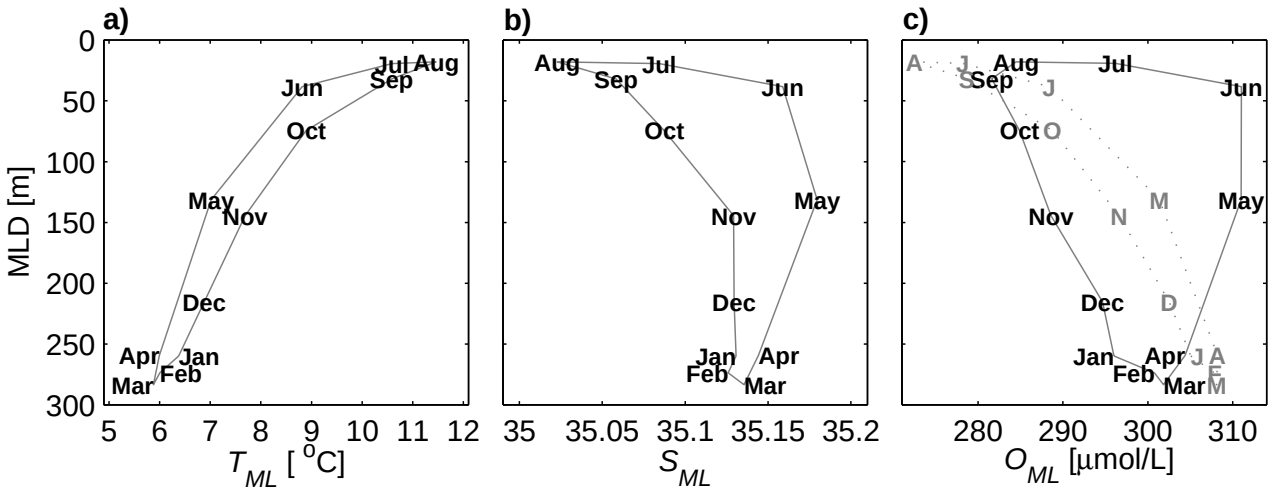

Figure 9: Hysteresis curves for the mean annual cycle of MLD in relation to a) ML-temperature, b) ML-salinity, and c) ML-oxygen concentration (full line) and ML-saturation concentrations (grey dotted line) at OWSM.

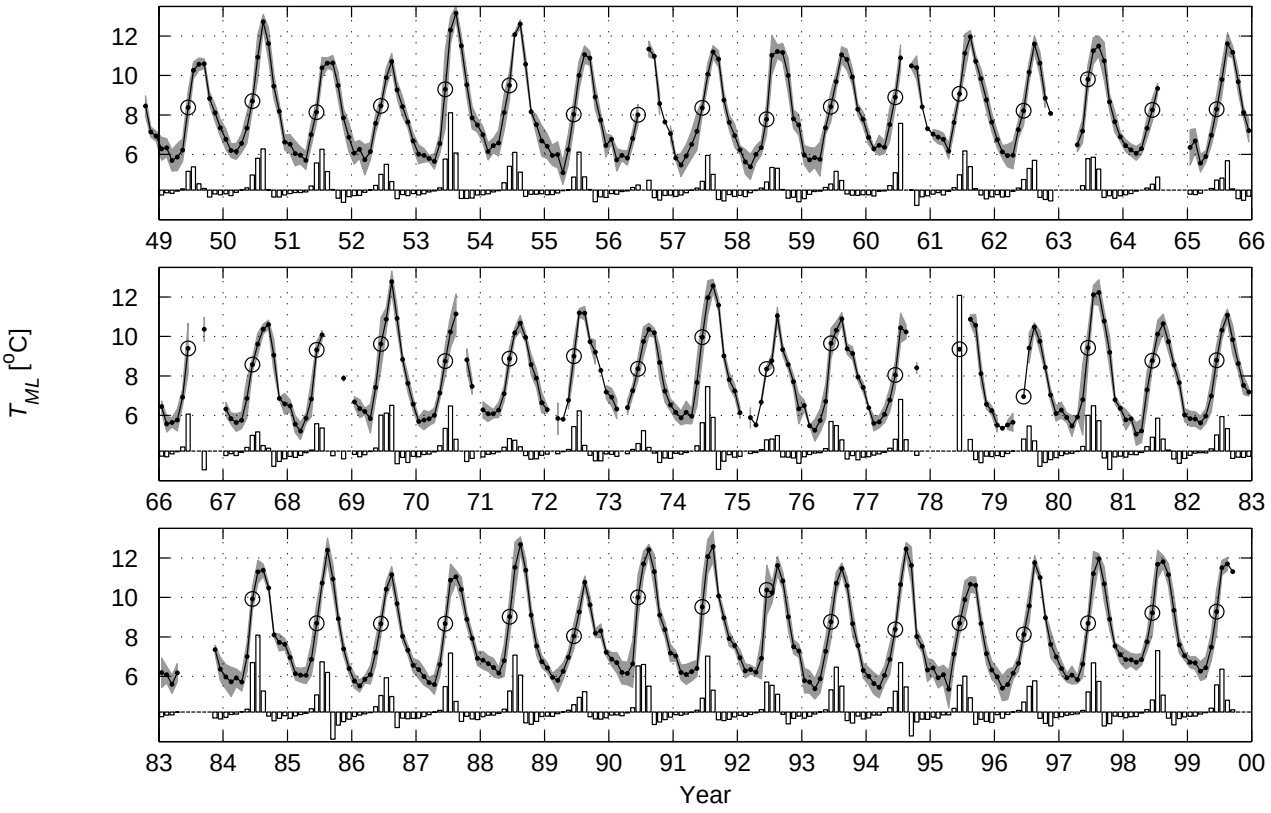

Figure 10: Monthly mean mixed layer temperature for the whole period (black line). Shading is explained in Figure 8. June months are circled. Bar graph shows surface warming of the mixed layer ($-Q/MLD$) and upward pointing bars are positive.

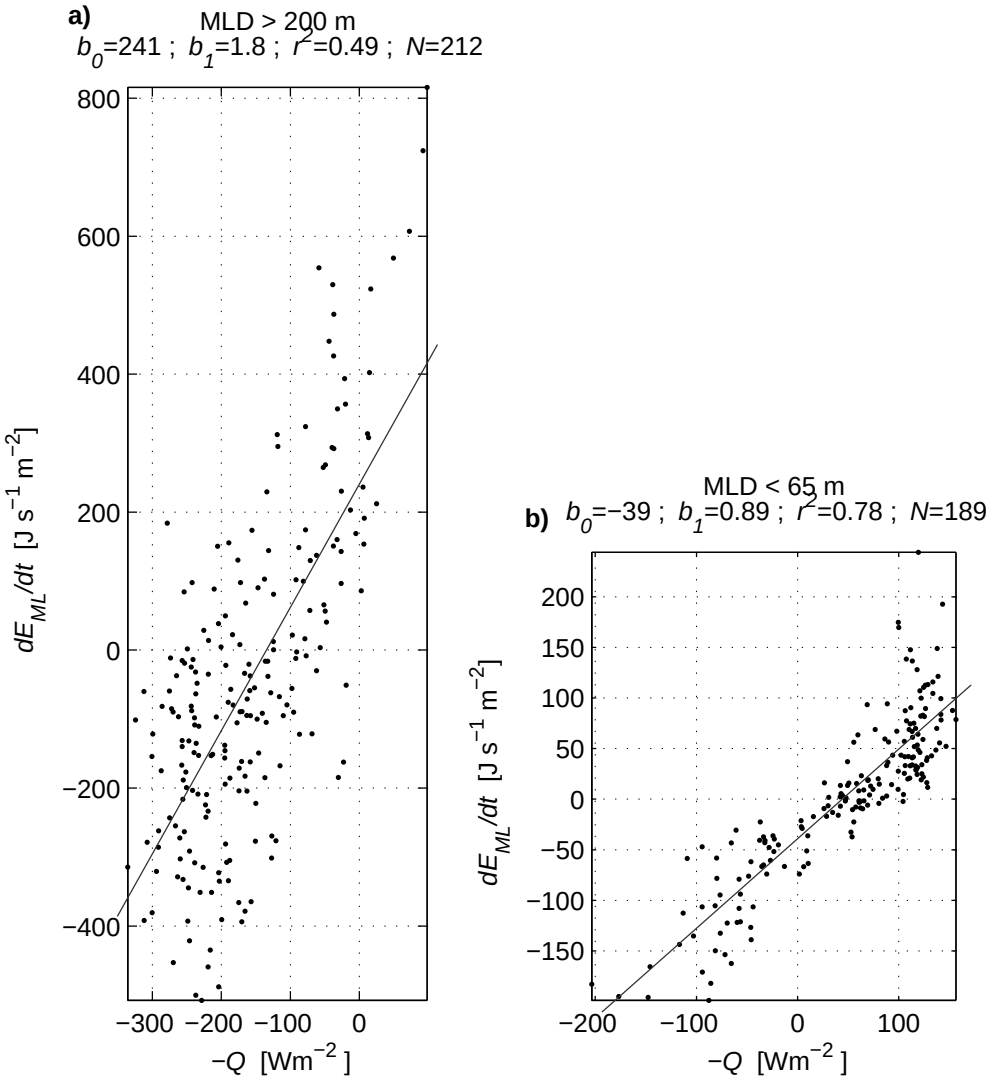

Figure 11: Monthly change in the mixed layer's heat content at OWSM as a function of local atmospheric heat flux for a) mixed layers deeper than 200 m and b) mixed layers shallower than 65 m. Linear regression lines for each case are added and regression statistics shown above the graphs (see text for explanation).

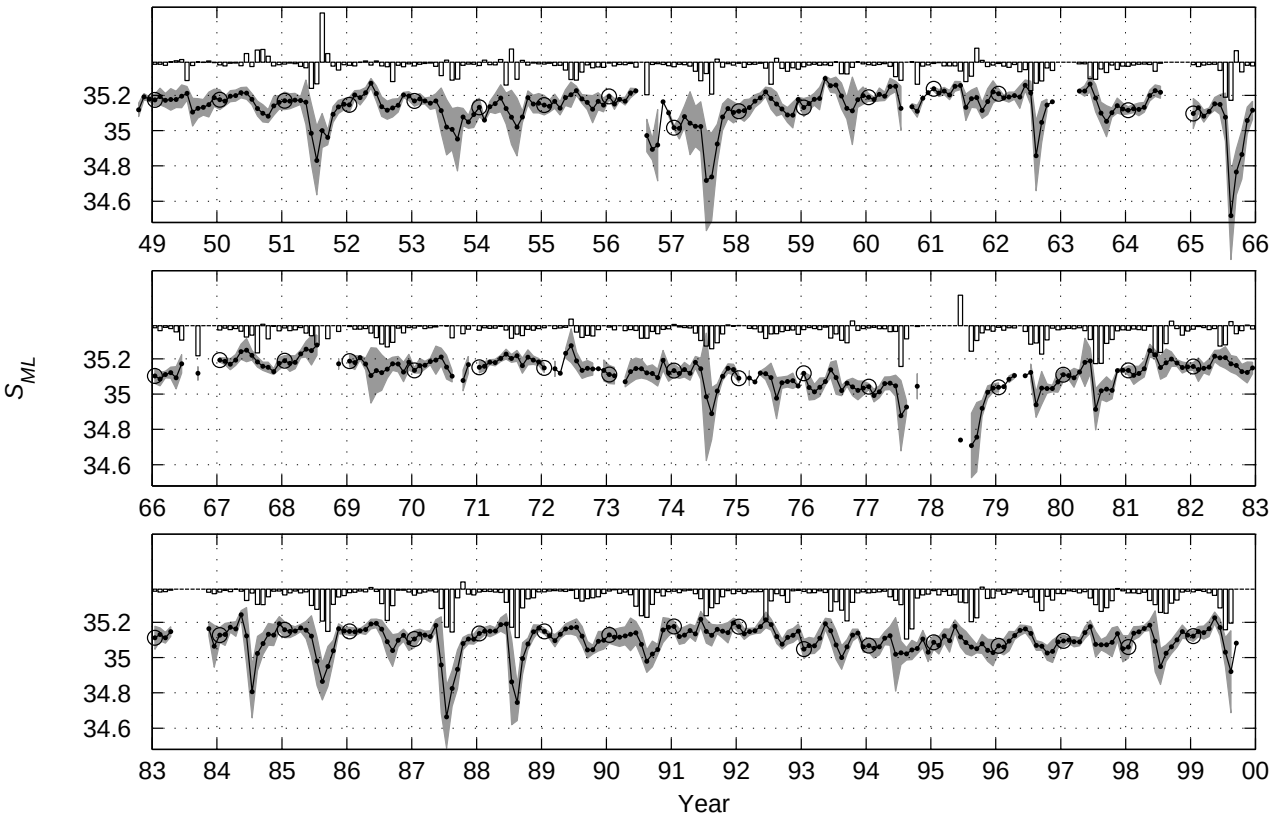

Figure 12: Monthly mean mixed layer salinity for the whole period (black line). Shading is explained in Figure 8. January months are circled. Bar graphs show contribution to salinity change by net freshwater *input* from the atmosphere ($(P-E)/MLD$). Upward pointing bars indicate *freshening*.

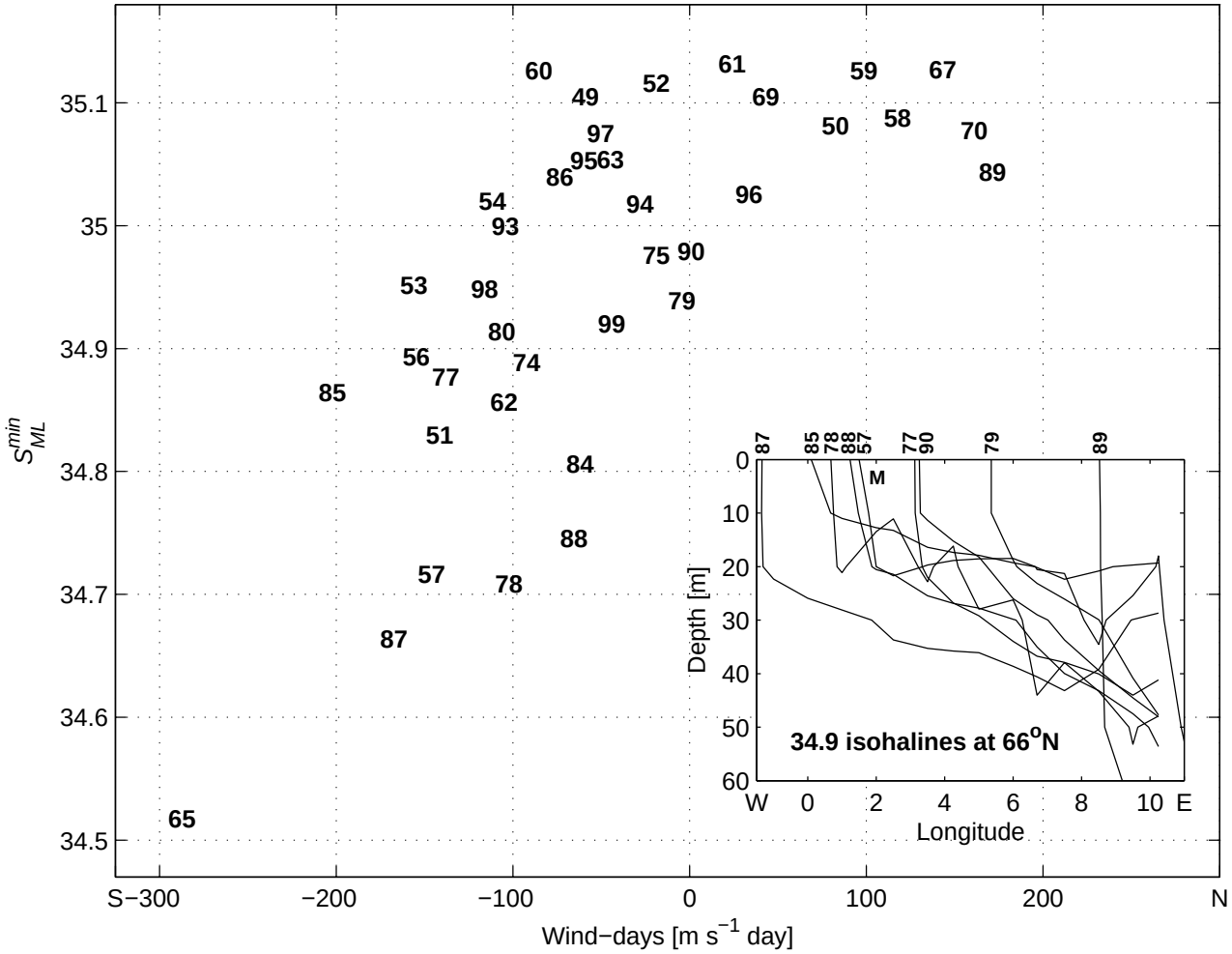

Figure 13: Northward component of wind integrated over time of development of salinity minima at OWSM, related to amplitude of these minima, for years with discernible summer minima. Numbers indicate years. The inlay shows the surface extrusion of fresher coastal water in AARI sections coinciding with salinity minima at OWSM.

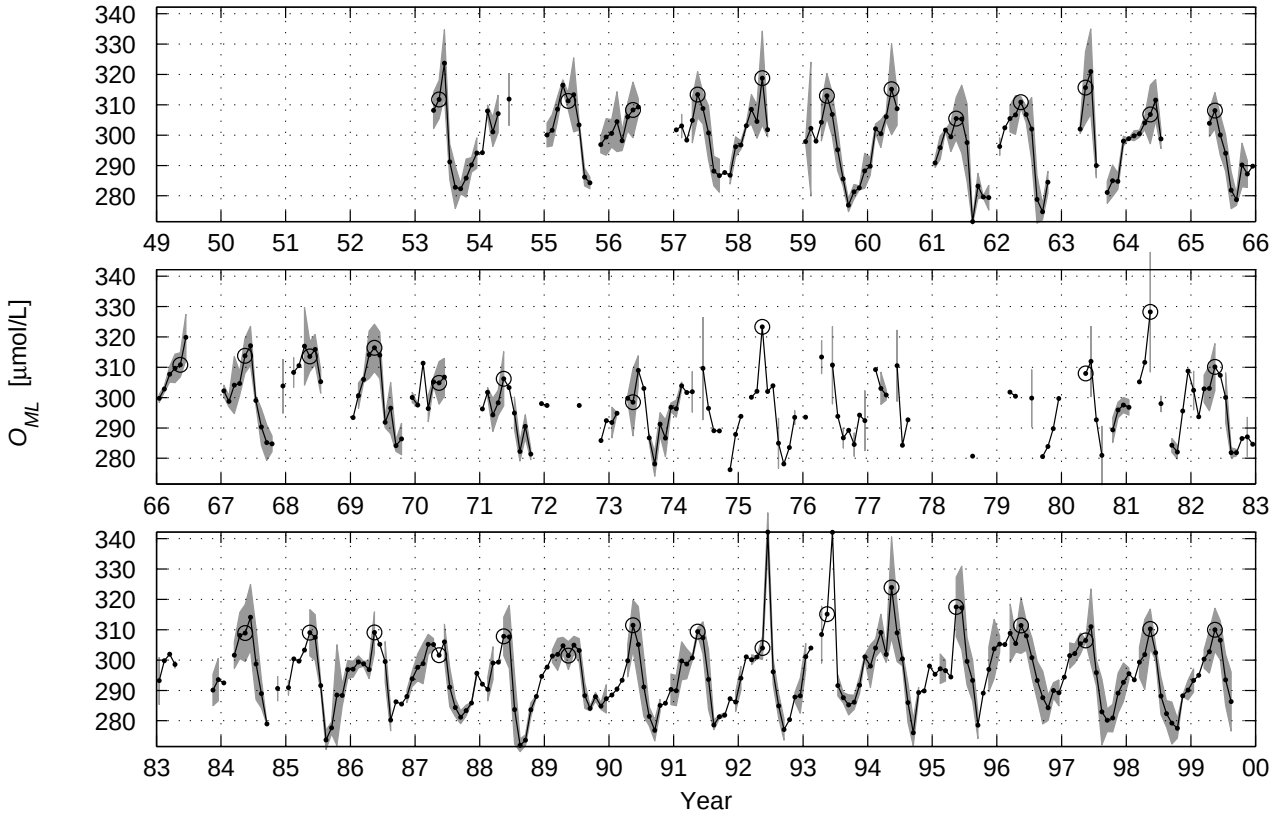

Figure 14: Monthly mean mixed layer oxygen concentration for the whole period (black line). May months are circled. Shading is explained in Figure 8.

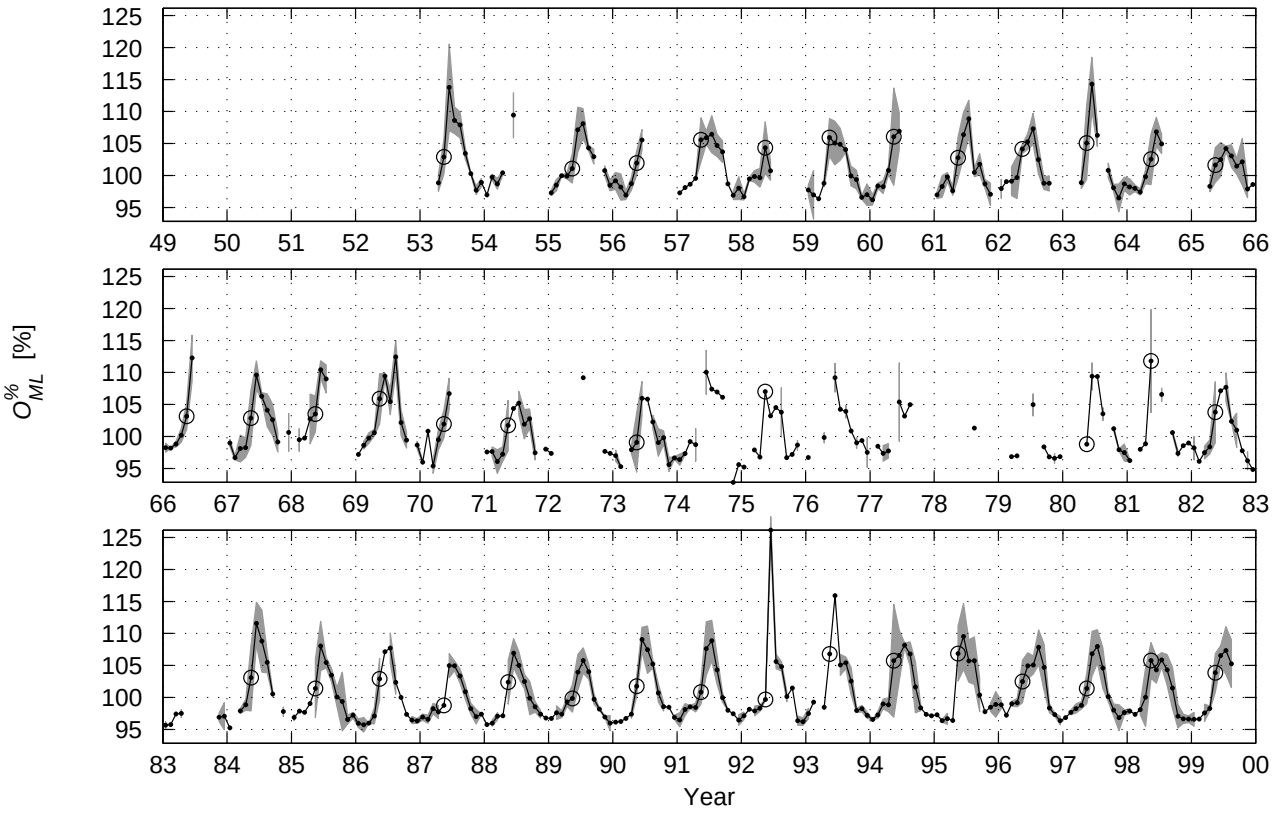

Figure 15: Monthly mean mixed layer percent oxygen saturation for the whole period (black line). May months are circled. Shading is explained in Figure 8.